cells

MDPI

Triphasic 3D *in vitro* model of bone-tendon-muscle interfaces to study their regeneration

Wendy Balestri[1], Graham J. Hickman[2], Robert H. Morris[3], John A. Hunt[4,5] and Yvonne Reinwald[1*]

[1]Department of Engineering, School of Science and Technology, Nottingham Trent University, Nottingham, UK
[2] Imaging Suite, School of Science & Technology, Nottingham Trent University, Nottingham, UK
[3]Department of Physics and Mathematics, School of Science and Technology, Nottingham Trent University, Nottingham, UK
[4]Medical Technologies and Advanced Materials, School of Science and Technology, Nottingham Trent University, Nottingham, UK
[5]College of Biomedical Engineering, China Medical University, Taichung 40402, Taiwan
[*]Author to whom correspondence should be addressed

Abstract: The transition areas between different tissues known as tissue interfaces have limited ability to regenerate after damage which can lead to incomplete healing. Previous studies focussed on single interfaces most commonly bone-tendon and bone-cartilage. Here, we develop a 3D *in vitro* model to study the regeneration of the bone-tendon-muscle interface. The 3D model was prepared from collagen and agarose, with different concentrations of hydroxyapatite to graduate the tissues from bone to muscle, resulting in a stiffness gradient. This graduated structure was fabricated using indirect 3D printing to provide biologically relevant surface topographies. MG-63, human dermal fibroblast and Sket.4U cells were found suitable cell models for bone, tendon, and muscle respectively. The biphasic and triphasic hydrogels composing the 3D model were shown to be suitable for cell growth. Cells were co-cultured on the 3D model over 21 days before assessing cell proliferation, metabolic activity, viability, cytotoxicity, tissue-specific markers, and matrix deposition to determine interface formations. The studies were conducted in a newly developed growth chamber that allowed cell communication while the cell culture media was compartmentalised. The 3D model promoted cell viability, tissue-specific marker expression and new matrix deposition over 21 days showing promise for the development of new interfaces.

Keywords: tissue interfaces; indirect 3D printing; 3D cell culture; co-culture; stiffness gradient; regenerative medicine; composite hydrogels

Citation Wendy Balestri[1], Graham Hickman[2], Robert H. Morris[2], John A. Hunt[3,4] and Yvonne Reinwald[1]. 2022, 12, x. https://doi.org/10.3390/xxxxx

Academic Editor(s):

Received: date
Accepted: date
Published: date

1. Introduction

In the musculoskeletal system, tissue interfaces transfer load from soft to hard tissues [1]. Interfaces have limited ability to regenerate after injuries and deterioration, which can prevent a complete healing of injuries and eventually lead to recurrence of the injury after treatment [2]. At present, treatments for repairing damage to musculoskeletal tissues involve surgical interventions, such as grafts and prosthetics to replace or augment the joint. However, these interventions do not aim to repair tissue interfaces [2,3]. The lack of interface regeneration might also lead to graft instability and limited implant-host integration, requiring the replacement of the implant few years after surgery. Tissue engineering approaches could be used to regenerate tissue interfaces to overcome these problems [4,5]. The biology of orthopaedic interfaces is widely known, but the mechanism behind their development is not yet fully understood.

Bone is a porous structure with pore sizes that increase from 10-50 µm (cortex bone) to 300-600 µm (trabecular bone). The bone matrix is made of 60% organic phase composed prevalently of type I collagen, and 40% of inorganic phase containing calcium,

phosphorous, sodium and magnesium which are organised in crystals and present in the form of hydroxyapatite (HA) ($Ca_{10}PO_4OH_2$) [1, 6–8]. The bone cell population includes osteoblasts, osteoclasts, and osteocytes.

Tendon is formed mainly of type I and type III collagen fibres, decorin, water and 0.2% of inorganic phase [9]. The cell type present in tendon is tenocyte. Bone and tendon are connected through the enthesis by mineralised and non-mineralised fibrocartilage [7]. Muscle is composed of bundles of myofibers, specialised multinucleated cells that derive from myoblasts. Each bundle is surrounded by ECM composed of type I collagen and proteoglycans [10,11]. Tendon and muscle are connected through the myotendinous junction by collagen extensions from the tendon ECM that join with the muscle fibres [1,7,12]. Currently, the focus is mostly on the regeneration of bone-tendon or bone-cartilage interfaces, with little investigation of the tendon-muscle junction [4]. Numerous studies investigate individual interfaces, while in the body multiple interfaces are involved in organ function [4,13] and typical injuries often involve more than one interface.

When interfaces are studied, it is important to develop gradient scaffolds that gradually change in composition, as well as physical or chemical properties [14]. Commonly, synthetic polymers like poly (lactic-co-glycolic acid) (PLGA) [5,15–17], poly (caprolactone) (PCL) [5,18–20] and poly (lactic acid) (PLA) [18,21–23] are used for enthesis studies. To the bone area, bio-glasses [15] or ceramics [16,19,24] can be added to resemble the inorganic phase. PCL is also used for MTJ studies [25,26]. The advantage of using synthetic polymers is their easy handling [27], however their bioactivity can induce an immune response when implanted [28]. Furthermore, their by-products can be toxic and cell adhesion is not always promoted [29]. Natural polymers do not induce an immune response and can promote cell adhesion and growth making them a more attractive choice. They can be used to coat the surface of synthetic scaffolds to improve cell adhesion, or they can be used to fabricate entire scaffolds. This, however, comes with reduced mechanical properties so natural polymers are often combined with other materials [27]. Collagen, for example, has been used as a 3D scaffold for a wide range of tissue engineering applications as it is the most abundant protein in the human body providing support to organs. Thirty different types of collagens are present in the body and some of these, such as collagen types I, III, V and XI have been applied clinically. Type I collagen is one of the most used for various tissues, including bone, tendon and muscle [30-33], as it does not induce an immune response [34]. Collagen has the suitable mechanical properties, but because covalent crosslinking is not present when it is employed in tissue engineering, it weakens. To increase its stability, physical, chemical, and natural crosslinkers can be used [35]. Alternatively, other biomaterials like chitosan [36] or agarose [37], [38] can be added to collagen to improve its mechanical properties. Collagen can also be mixed with calcium phosphates [39] or HA [40-42], to mimic mineralized tissues.

In vitro scaffolds should mimic the structure of the ECM. The surface topography, roughness, and elasticity of the substrate [30–32] influence cell responses including cell adhesion, proliferation, migration, morphology, differentiation, and gene expression. Nanopits have been shown to improve the expression of bone-specific markers in human mesenchymal stem cells (hMSCs) [46]. In 2016, Choi et al. increased the scaffolds' stiffness and improved MG-63 proliferation by adding HA to poly lactic-co-glycolic acid (PLGA) scaffolds [47]. Proliferation rate and APL activity was also increased when bovine osteoblasts were seeded on porous PCL scaffolds containing HA [48]. The nanofibrous PCL/gelatin scaffolds designed by Leong et al. promoted human dermal fibroblast proliferation and new matrix deposition over 28 days of culture [49]. In another study, PCL nanofibrous scaffolds enhanced human tenocytes' metabolic activity, alignment along the fibres and matrix production over 14 days [50]. The microgrooved collagen scaffolds developed by Chen et al. promoted the formation of muscle myofibers, myoblast alignment and the synthesis of new muscle ECM [51]. Myoblasts differentiated into myotubes with enhanced proliferation, elongation, alignment, and expression of muscle-specific markers when

cultured on fibrous PEG scaffolds [52]. Co-culture in interface studies requires an optimized approach [25, 40, 41] such as direct co-culture, where different cell types are seeded on the same substrate and cultured in the presence of a medium that promotes the survival of all the cell populations [54]. Cooper et al., co-cultured mouse fibroblasts and osteoblasts on a scaffold for enthesis regeneration. To promote high mineralization in the osteoblasts and low mineralisation in the fibroblasts, the optimal concentration of beta-glycerophosphate, the mineralizing agent, was added to basal medium supplemented with ascorbic acid, foetal bovine serum and antibiotics/antimycotic [21]. In 2015, Merceron et al. developed a differentiation media by adding horse serum, insulin–transferrin–selenium, ascorbic acid, aprotinin, and antibiotic/antimycotic to basal medium to allow the growth of C2C12 and NIH/3T3 [25]. Since the identification of the most appropriate supplements for different cell populations is time-consuming and costly [54] a device that allows cell-cell communication while each cell type is cultured in its specific medium should be developed. A silicon bioreactor, made of two chambers, separated by a perforated wall, was developed by Harris et al. in 2017. MSCs were seeded on a hydrogel that was placed in the perforated wall between the chambers. Endochondral or ligament differentiation was promoted by adding distinct differentiation media to each of the chambers [55]. To allow articular cartilage repair, Chang et al. optimized a dual-chamber bioreactor that promoted separation between chondrogenic and osteogenic medium using a silicon membrane that also contained the scaffold [56]. In interface studies, cells' phenotype, genotype or a combination of both at the interfaces are frequently inadequately investigated or entirely disregarded [23,44–46], with studies performed employing culture periods which are too short [25,47–49].

In this study, we aimed to develop a 3D *in vitro* model of bone-tendon-muscle to study the regeneration of both interfaces. For this purpose, a collagen/agarose-based composite hydrogel was developed, with a stiffness gradient generated by adding different concentrations of hydroxyapatite (HA). Therefore, the 3D *in vitro* model was fabricated by indirect 3D printing. A biologically relevant surface topography was designed, consisting of pores for the bone and ridges to mimic the tendon and muscle fibres. Human osteoblast-like cells MG-63, human dermal fibroblast, and Sket.4U were investigated to assess their suitability to be used as bone, tendon, and muscle cell models, respectively. After investigating suitable cell seeding densities for each cell type, cells were cultured individually on the newly developed hydrogels to assess their biocompatibility. The response of cells co-cultured on the 3D *in vitro* model in a newly developed growth chamber keeping the cell culture media separated while cells were in communication was assessed over 21 days.

2. Material and Methods

2.1. Preparation of biphasic and triphasic composite hydrogels

Agarose (Fisher Scientific, UK) was mixed with water to a final concentration of 0.75% (w/v) with different concentrations of hydroxyapatite (HA) nanoparticles (Sigma-Aldrich, UK), namely 0% (v/v) for the muscle area, 0.2% (v/v) for the tendon area and 40% (v/v) for the bone area. Type I rat tail collagen (Corning, UK) was prepared following the company's instruction to a final concentration of 3 mg/ml. Therefore, the required volumes of sterile 10x phosphate buffer saline (PBS), sterile 1N sodium hydroxide (NaOH) (Fisher Scientific, UK) in distilled water (dH_2O) and agarose/HA solutions were calculated and mixed for each section in individual tubes. To avoid too rapid polymerization of agarose, the solutions were kept in a water bath at 37°C. Additionally, collagen was kept at 4°C and added last to the mixture. After polymerization, bone and tendon triphasic gels were crosslinked with 10% (v/v) oligomeric proanthocyanidins (OPC) in 1x PBS for 60 minutes at 37 °C and 5% CO_2. The resultant hydrogels are listed in **Error! Reference source not found.**.

Table 1. Composition of biphasic and triphasic hydrogels.

Type of hydrogel	Collagen (mg/ml)	Agarose (% w/v)	Hydroxyapatite (% v/v)	Crosslinked
Biphasic (muscle)	3	0.75	0	No
Triphasic (tendon)	3	0.75	0.2	Yes
Triphasic (bone)	3	0.75	40	Yes

2.2. Determining Young's modulus from compression testing

To perform compression testing, biphasic and triphasic composite hydrogels were cut with a mould to obtain 2 mm thick discs of approximately 6 mm diameter. Compression tests were performed with the ElectroForce 3200 (TA instruments, USA) using a 1 N load cell applying a maximum displacement of 0.2 mm. For each sample, a load (F) vs displacement (δL) curve was plotted. Stress (σ) and strain (ε) were calculated using equations 1 and 2 respectively and used to plot the stress vs strain curves facilitating the calculation of Young's modulus (E) using equation 3 where the stress over strain parameter is determined from the linear fit of the plotted data.

$$\sigma = \frac{F}{A} \text{ (N/m}^2\text{)}, \quad (1)$$

$$\varepsilon = \frac{\delta L}{L}, \quad (2)$$

$$E = \frac{\sigma}{\varepsilon} \text{ (N/m}^2\text{)}, \quad (3)$$

where A is the cross-sectional area of the sample and L is the initial sample thickness.

2.3. Design and fabrication of the 3D in vitro model

The 3D *in vitro* model was designed with Autodesk Fusion 360 (version 2.0.12392). The model comprises three sections, each with biologically relevant surface topography. A pore gradient was designed for the bone section, and ridged structures to encourage fibres for the tendon and the muscle sections (**Error! Reference source not found.**A). The model was fabricated by indirect 3D printing using a mould (Figure 1B), comprised of a base to prevent the hydrogel leakage (1), a support with the negative shape of the 3D *in vitro* model (2), a main body providing a rectangular shape (3) and a lid to prevent bacterial contamination during hydrogel polymerization. The mould was fabricated with stereolithographic 3D printing (Form 2, Formlabs, USA), in clear resin (base and support, F2-GPCL-04) and tough resin (body and cover, FL-TOT-L05) resin (Formlabs, USA). The parts of the mould were washed and cured after printing to remove uncured resin. The mould was then autoclaved for 20 minutes at 120 °C. To facilitate the removal of the hydrogel after polymerization, the mould was immersed overnight at 4 °C in sterile 1% (w/v) Pluronic ® F-127. The mould was then assembled, and the triphasic bone gel, the triphasic tendon gel and biphasic muscle gel were added to the assembled vertical mould and allowed to polymerize in a sterile glass beaker for 60 minutes at 37 °C and 5% CO_2. To crosslink the bone and tendon triphasic gels, the mould's base and support were removed. The body of the mould was placed in a 3D printed sterile bottle with 3 ml of crosslinker for 60 minutes at 37 °C and 5% CO_2.

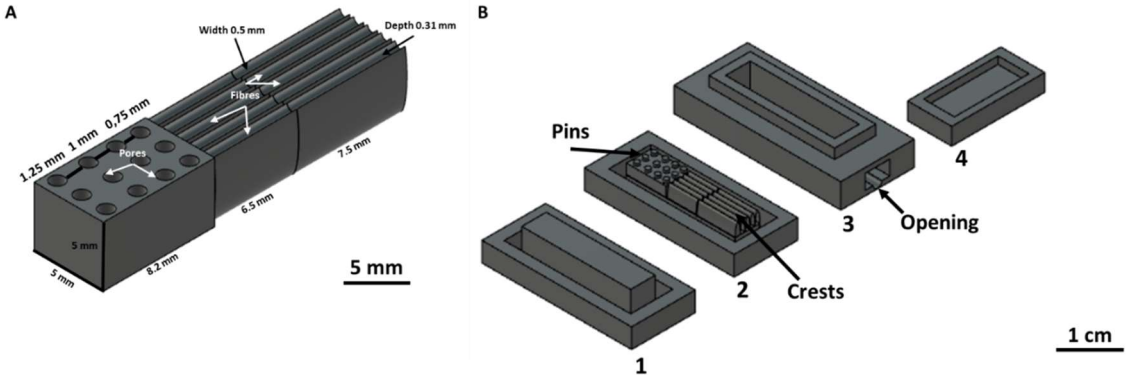

Figure 1. CAD model of the 3D *in vitro* interface model and vertical mould A) The 3D model was designed with Autodesk fusion 360 with pores (bone section) and ridges (tendon, muscle sections). B) A vertical mould for fabricating the 3D *in vitro* model was made of a base (1), a support with the negative shape of the surface topography (2), a body to provide the main rectangular shape of the model (3) and a lid to prevent bacterial contamination (4).

2.2 Energy Dispersive Spectroscopy (EDS) with Scanning Electron Microscope (SEM)

To assess the chemical composition, the 3D *in vitro* model was placed in a freeze-dryer (Christ Alpha 1-2 LDplus, Premier Scientific, UK) at -60 °C and 0 mbar, for 8 hours. For SEM/EDS analysis, samples were mounted on adhesive carbon tape and coated with 5 nm Au using a Quorum Q150R coater to minimise charge effects. Sample morphology was visualised by secondary electron imaging using a JEOL JSM7100F LV FEGSEM operating at 5.0 kV and a working distance of 10 mm. Qualitative energy dispersive spectroscopy mapping was performed at 20 kV with an Oxford Instruments XMaxn 80 mm^2 silicon drift detector to determine the elemental distribution with assignments and data export performed using Oxford Instruments Aztec software (version 3.3 SP1).

2.3. Fabrication of the co-culture growth chamber

The model was cultured within a growth chamber which comprised a body and a lid. The chamber body was composed of three compartments, one for each tissue, separated by barriers with an opening allowing the placement of the 3D *in vitro* model and cell communication. To keep each cell culture medium in its compartment, barriers were also present on the lid. Inlets and outlets were designed to allow the connection of a peristaltic pump providing a dynamic flow of media to the cells. Leakage and medium isolation tests were performed by adding water stained with different food colours to the compartments.

To assess the biological inertness of the resin, MG-63 were seeded on the bottom of the chamber. After 24 hours, haematoxylin and eosin (H&E) stain was performed to verify cell adhesion to the chamber. H&E stain was also performed on a chamber without cells (negative control) and MG-63 seeded on a 24-well plate (positive control).

2.4. Response of cells cultured on 3D hydrogels

MG-63 (ATCC®, USA), human dermal fibroblast (HDF) (ATCC®, USA) and Sket.4U cells (Axiogenesis, DE) were expanded in 2D. For MG-63 and HDF, high-glucose DMEM (Gibco™, Thermo Fisher Scientific, UK) was supplemented with 10% Foetal Bovine Serum (FBS) (Gibco™, Thermo Fisher Scientific, UK), 1% L-glutamine (L-Glu) (Gibco™, Thermo Fisher Scientific, UK) and 1% penicillin/streptomycin (P/S) (Gibco™, Thermo Fisher Scientific, UK). For the Sket.4U a Skeletal muscle cell medium (Sigma-Aldrich, UK) was used.

To identify cell seeding densities where cells reached homeostasis in 3D, MG-63, HDF, and Sket.4U were seeded with a concentration of 5,000 cells/gel (MG-63), 50,000 cells/gel (HDF) or 100,000 cells/gel (Sket.4U) on biphasic gels. Cells were seeded

simultaneously on the 3D *in vitro model*. The model was then placed in the growth chamber and incubated at 37 °C in 5% CO_2 for 3 hours to allow cells to adhere to the model. Then the chamber was filled with complete medium in the bone section, complete medium in the tendon section and skeletal muscle medium in the muscle section.

On days 1, 3, 7, 14, and 21, DNA content, metabolic activity, cell morphology, and expression of tissue-specific markers were assessed with PicoGreen assay (Invitrogen™, Thermo Fisher Scientific, UK), Alamar Blue assay (ThermoScientific™, Thermo Fisher Scientific, UK), histology, and immunocytochemistry respectively. All assays were performed following the manufacturers' instructions.

2.5. PicoGreen assay

At each time point, samples were collected and stored in 0.5 mg/ml Proteinase K (Thermo Fisher Scientific, UK) in 100 mM ammonium acetate (Sigma-Aldrich, UK) at -80 °C until the assay was performed. Then samples were defrosted and incubated overnight at 60 °C to digest the samples. Fluorescence was read with an excitation of 480 nm and emission of 520 nm using Varioskan Lux 3020 spectrophotometer (Thermo Fisher Scientific, UK). For the 3D interface model and co-culture n=24 was determined.

2.6. Alamar Blue

At each time point, the medium was removed, and samples were incubated with the Alamar blue (Thermo Fisher Scientific, UK) working solution for 3 hours at 37°C and 5% CO_2. The solutions were then transferred to a 96-well plate and the absorbance was read spectrophotometrically at 570 nm and 600 nm (Varioskan Lux 3020 spectrophotometer, ThermoFisher Scientific, UK). For the 3D interface model and co-culture n=36 was determined.

2.7. LIVE/DEAD™ Viability/Cytotoxicity Kit

Cell viability was assessed for cells co-cultured on the 3D *in vitro* interface model with Live/Dead™ (Invitrogen™, UK). The 3D *in vitro* model was placed in a glass bottom dish 35 mm (Ibidi®, DE), and the working solution was added to the plate for 30 minutes at room temperature (RT) in the dark. After incubation, cells were imaged with a confocal microscope (Leica, DE). Z-stacks of each section were performed, and 3D projections were created with ImageJ.

2.8. LDH Cytotoxicity Assay

Cell cytotoxicity was assessed for cells co-cultured on the 3D *in vitro* model with Lactate dehydrogenase (LDH) Cytotoxicity assay (Invitrogen™, UK). Cell culture medium was collected at different time points and stored at -80°C until the assay was performed. Absorbance was read at 490 nm and 680 nm (n=9).

2.9. Immunocytochemistry

The expression of tissue-specific markers was assessed with immunocytochemistry. All primary and secondary antibodies were obtained from Abcam (Cambridge, UK) unless otherwise stated and 4',6-diamidino-2-phenylindole (DAPI) was obtained from Sigma-Aldrich (UK). Samples were fixed with 10% formalin (Sigma-Aldrich, UK) for 30 minutes at RT. Then, cells were permeabilized with 0.1% (v/v) Triton-x (Alfa Aesar™, UK) in PBS for 5 minutes. After washing cells three times with dH_2O, 5% (w/v) bovine serum albumin (BSA) in 1x PBS was added for 30 minutes at RT for blocking. Primary antibodies were diluted in 1% (w/v) BSA to a final concentration of 1:100 for osteonectin and tenomodulin; and 1:500 for α-SMA. Solutions were added for 60 minutes at RT. Secondary antibodies and DAPI were diluted 1:1000 in 1% (w/v) BSA. Cells co-cultured on the 3D in vitro model, Donkey Anti-Rabbit IgG H&L (Alexa Fluor® 647) was added to osteonectin,

Goat Anti-Rabbit IgG H&L (Alexa Fluor® 488) was added to tenomodulin, and Donkey Anti-Rabbit IgG H&L (Alexa Fluor® 555) was incubated with Alpha-SMA for 60 minutes at RT in the dark. DAPI was incubated for 15 minutes at RT in the dark. Cells were imaged with a Leica SP5 confocal microscope (Leica, DE). Z-stack of each section were performed, and 3D projections were created with ImageJ.

2.10. Histological staining

Cell morphology and matrix deposition were assessed with histological stains. For comparison with native orthopaedic interfaces, mouse joints were sectioned and stained. All samples were fixed with 10% formalin (Sigma-Aldrich, UK) for 30 minutes. Mouse limbs were decalcified for 8 days in 8% HCl (Fisher Scientific, UK) in dH_2O and 8% formic acid (Alfa Aesar™, UK) in dH_2O at a ratio of 1:1, at 4 °C. The solution was changed every 2-3 days.

The dehydration of the 3D *in vitro* model and mouse limbs was performed with Excelsior™ ES Tissue Processor (Thermo Scientific™, UK). Briefly, samples were incubated in 70% ethanol, 80% ethanol and 95% ethanol for 60 minutes each at RT. Then, samples were incubated in xylene for 60 minutes three times at RT and in paraffin wax at 60 °C for 80 minutes three times. Embedding in paraffin was performed with HistoStar™ Embedding Workstation (Thermo Scientific™, UK). Samples were sectioned using a microtome (Leica RM2235, DE), with a thickness of 7 μm. Cells and sections were stained at room temperature using Alizarin red and haematoxylin and eosin stains (H&E). Briefly, 1% (w/v) alizarin red was dissolved in dH_2O. The pH was adjusted to 4.1~4.3 with 10% sodium hydroxide (Fisher Scientific, UK). Cells cultured on the 3D *in vitro* models and mouse limbs were stained for 60 minutes. For H&E stain, haematoxylin was added for 15 minutes. Then eosin Y was added for up to 2 minutes. The slides were dehydrated in ethanol 80% and 95%, each for 1 minute, then twice in 100% ethanol for 3 minutes. Slides were incubated twice in xylene for 10 minutes before being mounted with DPX mounting medium (Thermo Scientific™, UK). Slides were then imaged at 4x and 40x magnification using the Leica ICC50 W (Leica, DE) microscope.

2.11. Statistical analysis

Statistical analysis was performed with IBM SPSS®. Data were analysed using One-way ANOVA followed by Tukey post-hoc test with a confidence interval of 99.99% (***), 99% (**) and 95% (*). Graphs were plotted with Microsoft Excel and statistical significance was added with Inkscape (Inkscape project).

3. Results

3.1. Fabrication of the 3D in vitro model and the growth chamber

The 3D *in vitro* interface model was designed with three sections with different surface topographies, namely pores with size gradient for the bone, and ridges and channels mimicking tendon and muscle fibres (**Error! Reference source not found.**A). To assess the formation of surface topographies, the mould was tested with different concentrations of agarose, namely 4% (w/v) (blue), 2% (w/v) (transparent) and 1% (w/v) (yellow). Each section was then imaged with a brightfield microscope (**Error! Reference source not found.**B). Top and lateral views of the surface topography showed that pores, and channels and ridges in the tendon section were well defined. In the muscle section, ridges and channels were shorter and not well defined, assumingly due to the lower agarose concentration used. Because type I collagen is the primary component of the bone, tendon and muscle matrix, it was chosen as the main biomaterial for the 3D model fabrication. However, collagen was not able to form a stable 3D model (data not shown). As stated above, agarose, on the contrary, was able to form the 3D model, thus collagen 3 mg/ml was mixed with 0.75% (w/v) agarose. This agarose concentration was selected because it was the

lowest concentration that provided sufficient support to collagen for the formation of the 3D interface model (data not shown). To assess the stiffness of the biphasic and triphasic gels, Young's moduli were determined by compression test. The values obtained were ~20 kPa for the muscle biphasic gels, ~140 kPa for the tendon triphasic gels and ~240 kPa for the bone triphasic gels, resulting in the desired stiffness gradient within the 3D *in vitro* interface model (**Error! Reference source not found.**C).

The growth chamber (Figure 3A) was able to keep three coloured liquids separated for 10 minutes (**Error! Reference source not found.**B), indicating the potential to separate tissue-specific media whilst enabling cell communication. The absorbance and the related dye concentrations were measured at 0 minutes, 10 minutes, and 60 minutes after their addition to the chamber (**Error! Reference source not found.**C). Although after 60 minutes the liquids mixed, the amount of mixing was considered acceptable, as in the body each tissue is not completely isolated from another, and a chemical gradient is normally present. The chamber prevented a complete mixing of the liquids after 24 hours (data not shown).

To assess the bio-inertness of the resin, MG-63 were seeded on the bottom of the chamber. No cells were observed in any of the chambers and cells were not expected to adhere to the chamber material. The absence of positive staining in both chambers suggested that the chamber is bioinert.

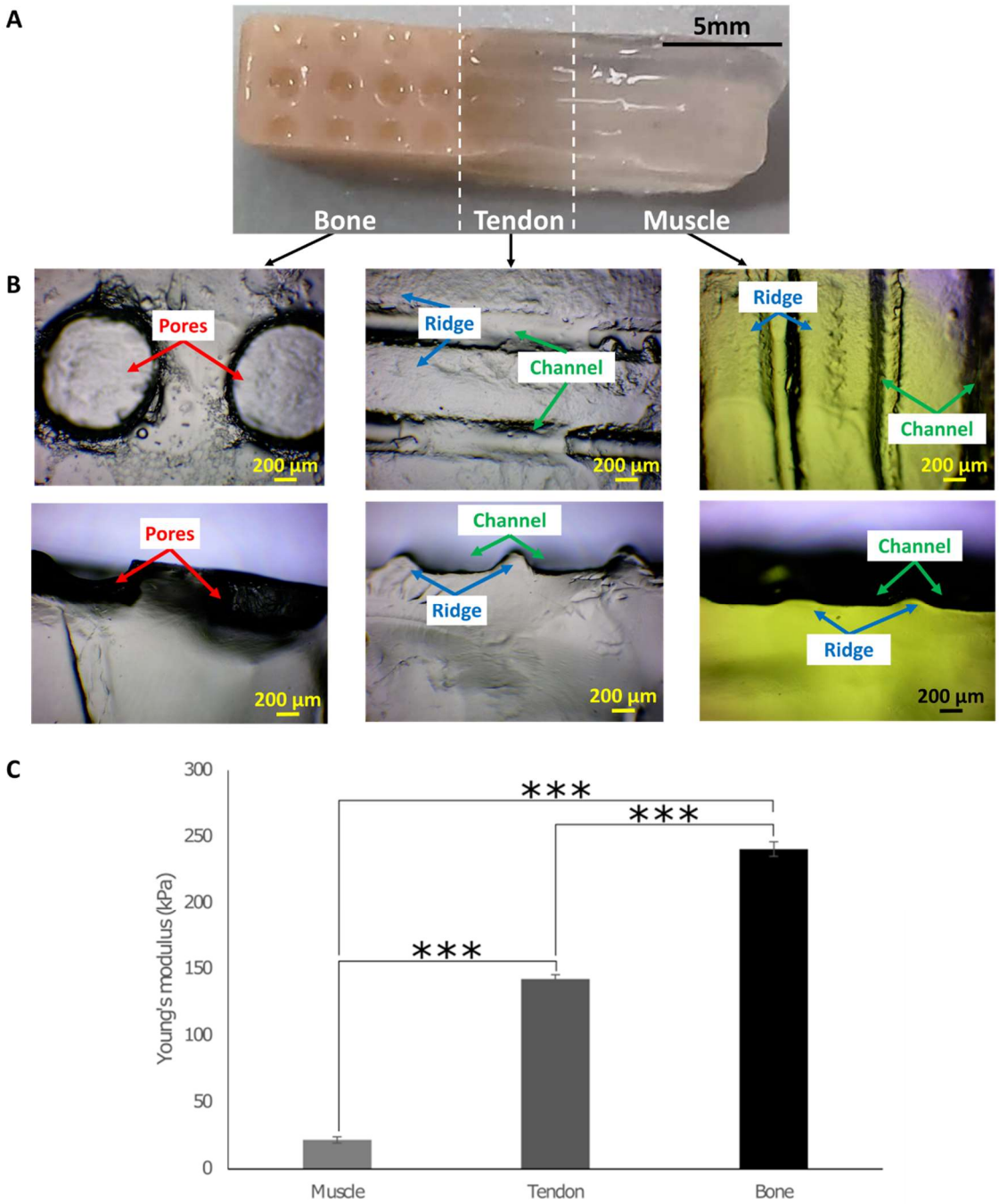

Figure 2. Surface topography and Young's moduli of the 3D *in vitro* model. A) The 3D *in vitro* model was made of three sections made of 3 mg/ml type I collagen, 0.75% (w/v) agarose and a gradient of hydroxyapatite decreasing from the bone to the muscle section. B) top and lateral views of the pores on the bone section; the ridges and channels of the tendon and muscle sections. Scale bar = 5 mm and 200 µm. C) Compression test was performed with 1N load cell. Young's modulus was determined from stress vs strain curves. A stiffness gradient was obtained with an increase of the Young's modulus from muscle to bone hydrogels. One-way ANOVA and Tukey post hoc test were performed, *= $p<0.05$, **=$p<0.01$, ***=$p<0.001$. Error bars show standard deviation (Muscle n=7; Tendon: n=6; Bone: n=5;).

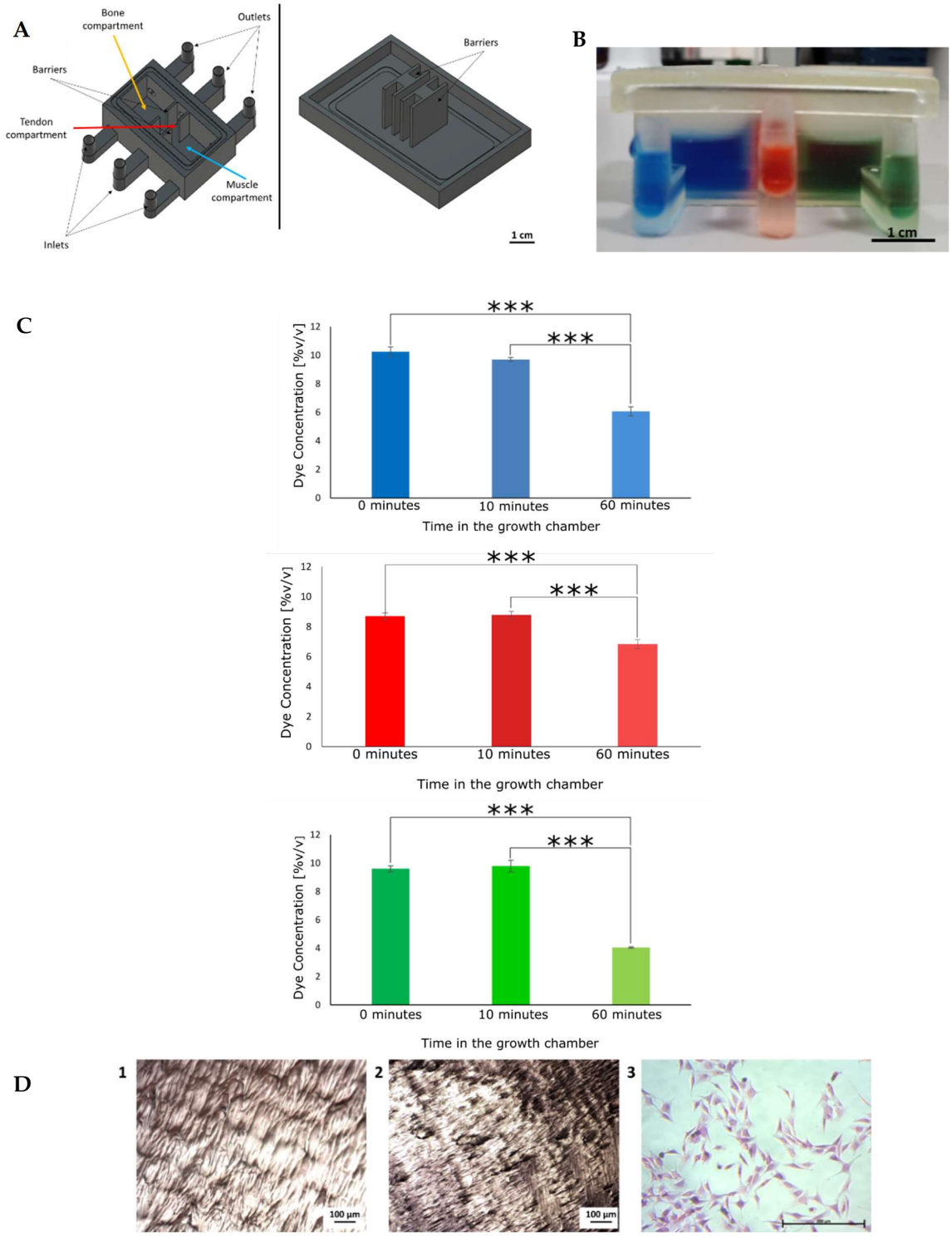

Figure 3. Fabrication and testing of the growth chamber. A) The growth chamber is composed of a body and a lid. The body is divided in three compartments, one for bone (yellow arrow), tendon (blue arrow), and muscle (red arrow). Both body and lid have barriers that keep the media separated. Media inlets and outlets were designed to allow for medium circulation. Scale bar = 1 cm. B). A gel was placed at the bottom of the chamber. Liquids in different colours were added to the chamber. After 10 minutes there was no sign of the liquids mixing. Scale bar = 1 cm. C) Concentrations for blue dye, red dye and green dye were determined. D) MG-63 were seeded on the chamber and stained after 24 hours. H&E stain of chamber without cells (1), chamber incubated with cells (2) and MG-63 cultured in 2D (3). MG-63 were imaged at 10x magnification. In both chambers there was no sign of cells on the bottom. Scale bar = 100 µm (1,2) and 200 µm (3).

3.2. SEM/EDS analaysis to assess hydrogels' composition

Figure 4 shows representative SEM images of the bone, tendon, and muscle sections. Secondary electron imaging (EDS electrons) shows that in all the sections there is the presence of crystals. Energy Dispersive Spectroscopy (EDS) suggests that many of the crystals are principally sodium chloride (NaCl). NaCl being a component of PBS, that was used to dilute collagen, as described in section 2.1, explaining why Na and Cl are abundant. A gradient of HA ($Ca_{10}PO_4OH_2$), decreasing from bone to muscle, was generated within the 3D model. Regions of Ca and P were observed by EDS mapping. Looking at the percentage of Ca and P present in the sections (Figure 5), it is possible to observe that the abundance of these elements decreases from bone to muscle, following the expected trend.

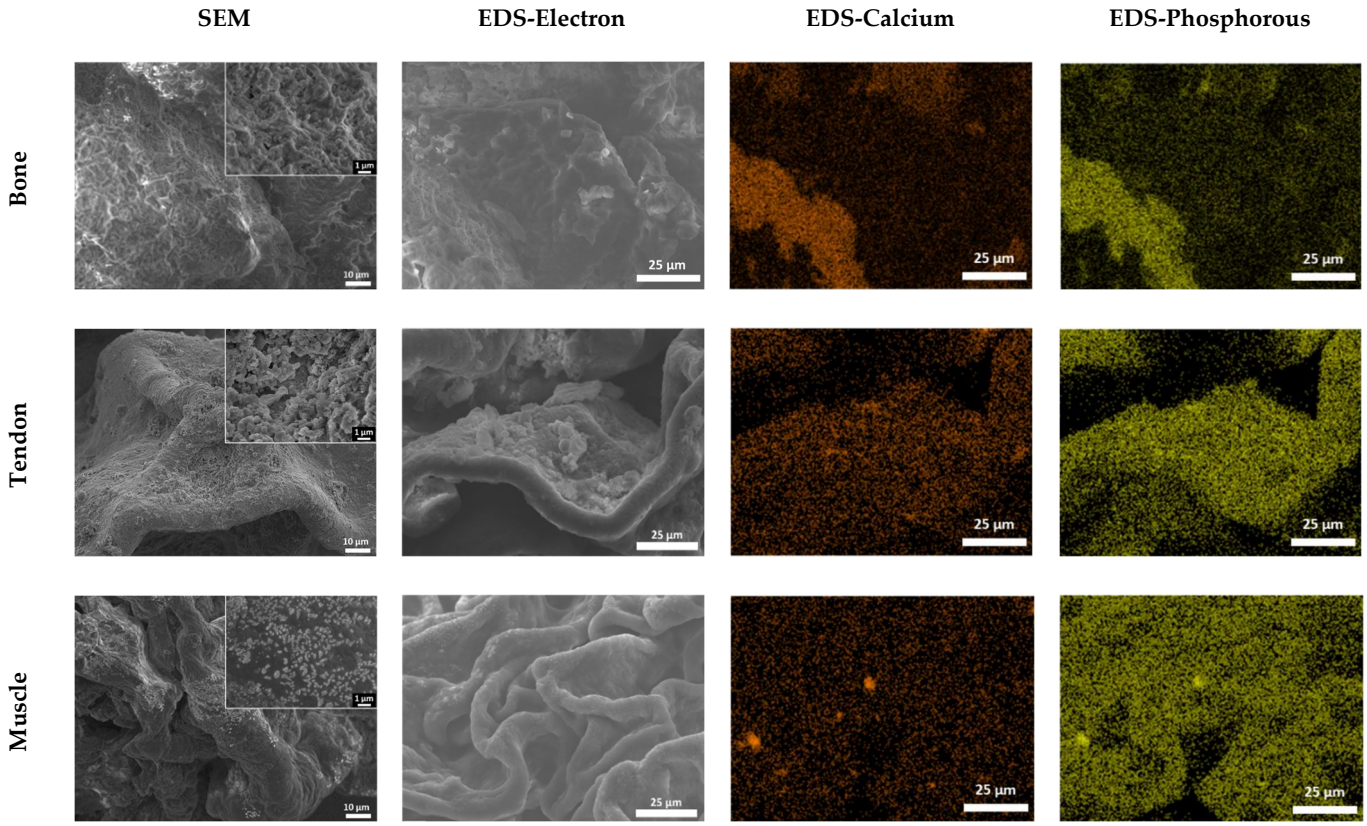

Figure 4. **SEM and EDS imaging of the 3D *in vitro* model.** Samples were freeze-dried for 8 hours and imaged with SEM. SEM images show the structure of the bone, tendon, and muscle sections at 1000x and 10,000x (inserts) indicated magnification. Scale bars = 10 µm for 1000x and 1 µm for 10,000x. EDS analysis shows the distribution of calcium and phosphorus within the sections. Images analysed at 1000x, scale bar 25 µm.

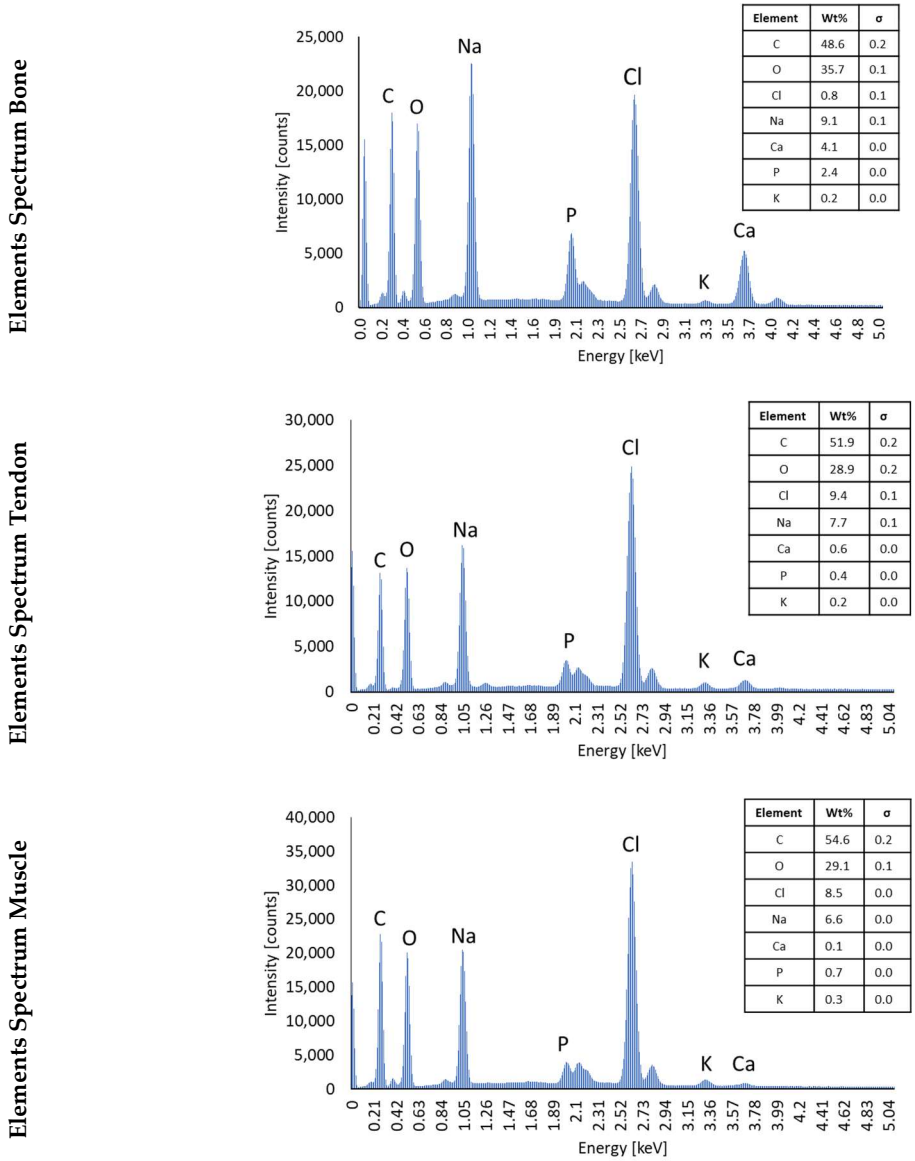

Figure 5. **EDS analysis of the 3D *in vitro* model.** EDS spectrum analysis indicates highest amounts of calcium were found in the bone and tendon section. Additionally, together with calcium and phosphorus, there are also high percentages of sodium and chloride.

3.3. Identification of cell homeostasis

Before cell culture experiments were carried out on the 3D hydrogels and interface model, MG-63, HDF and Sket.4U were assessed in 2D culture for their suitability to act as cell models for bone, tendon, and muscle, respectively (supplementary data, Figure S1, S2).

Cells were then seeded on the 3D hydrogels to identify which seeding densities are required for cells to reach homeostasis. This is the point, cells will stop proliferating, and start to migrate, and to produce new matrix to eventually form the interfaces.

Concentrations of 5,000 cells/gel, 50,000 cells/gel and 100,000 cells/gel were seeded on biphasic gels. DNA content and metabolic activity were assessed with PicoGreen assay (Figure 6A) and Alamar blue (Figure 6B), respectively. Cells cultured at 5,000 cells/gel did not reach homeostasis, as the DNA content of cells continued to increase with time. The DNA content of 50,000 cells/gel (MG-63) remained stable between days 3 and 7 before increasing to day 14 though not significantly for 100,000 cells per gel. For HDF, the DNA content remained similar for all seeding densities until day 3, where cell numbers were lower compared to day 1. For 50,000 cells/gel the DNA content increased again between day 7 and 14. For 100,000 cells, the DNA content increased by day 7 and then remained stable until day 14. For Sket.4U, the DNA content for 50,000 cells/gel decreased by day 3 and did not increase significantly for 100,000 cells/gel per gel. For both cell densities, DNA content decreased between day 7 and 14. For all cell types and seeding densities, the metabolic activity at day 14 was not statistically different in comparison to day 1 (except Sket.4U 50,000 cells per gel where it decreased). For MG-63 and HDF, metabolic activity on day 3 was higher than on day 1. No differences were seen for Sket.4U. For MG-63, 50,000 cells/gel and Sket.4U 100,000 cells/gel no statistical differences were observed between day 3 and day 7. The metabolic activity decreased at day 14 insignificantly for Sket.4U 100,000 cells/gel. The remaining seeding densities, showed significant differences between day 3 and 7, followed by a decrease by day 14.

Since MG-63 showed a higher growth rate than the other cells when cultured in 2D and on biphasic gels, 50,000 cells/gel was chosen as the most suitable cell seeding density. Because the DNA content for HDF increased for both seeding densities and the metabolic activity was not statistically different until day 14, 50,000 cells/gel was selected as cell seeding density. The DNA content of Sket.4U for 50,000 cells/gel and 100,000 cells/gel were similar, indicating that fewer cells were more metabolically active. However, 100,000 cells/gel was chosen as cell seeding density due to the lack of fibre formation in 2D culture.

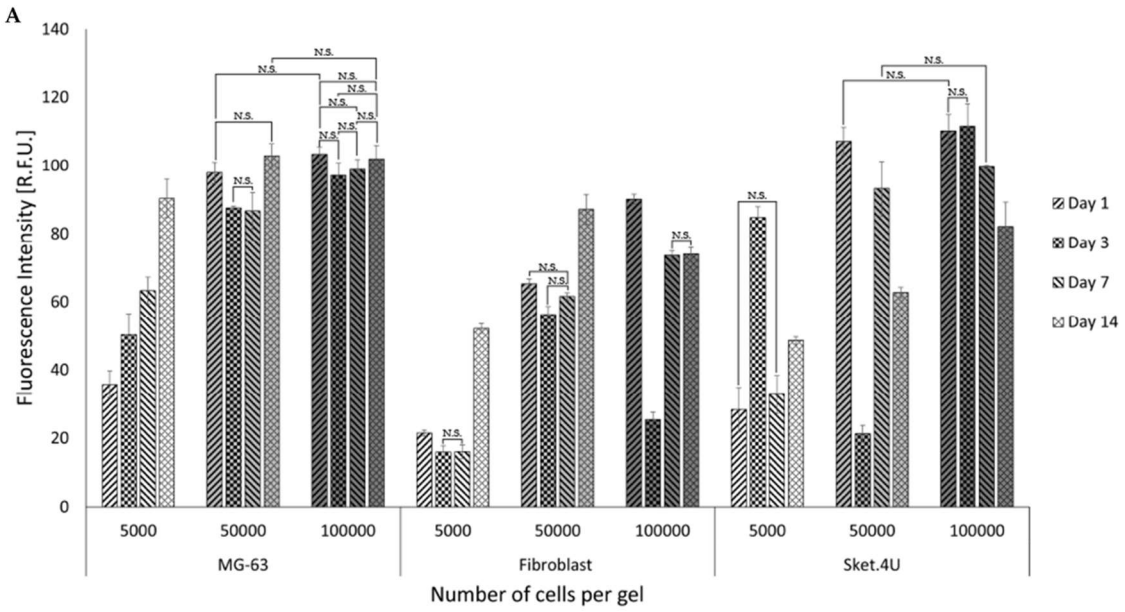

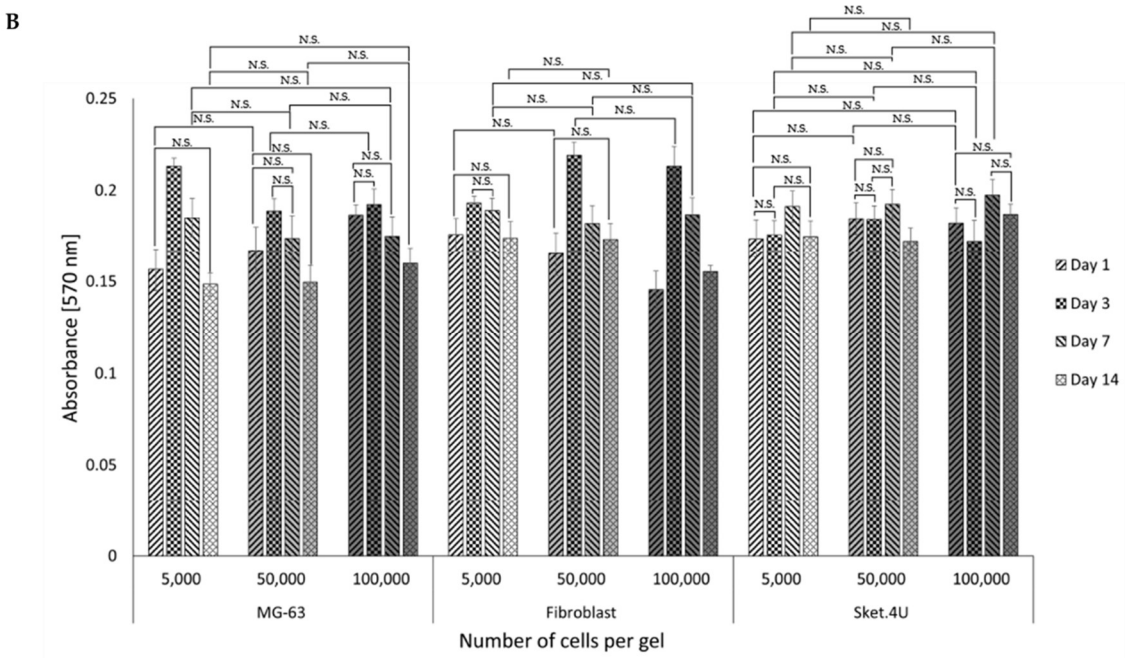

Figure 6. DNA content and metabolic activity assessed for cells grown on biphasic hydrogels. Cells were seeded with a cell density of 5,000 cells per gel, 50,000 cells per gel or 100,000 cells per gels in a 96 well plate to assess homeostasis. On day 1,3,7 and 14 after seeding A) DNA content was quantified using PicoGreen assay and fluorescence intensity was read at excitation 480 nm and emission 520 nm (n = 6); B) Alamar Blue assay was performed and the absorbance was read at 570 nm and 600 nm (n=9). Multi-way ANOVA and Tukey post hoc test were performed. N.S = not significant, the other values are statistically significant with $p<0.05$. Error bars show standard deviation. The increase of colour intensity indicates the cell seeding density, the pattern represents the time point.

3.4. Biocompatibility of biphasic and triphasic gels

Cells were seeded individually on the biphasic and triphasic gels at the previously identified cell seeding densities, namely MG-63 were seeded on triphasic gels at 50,000

cells/gel; HDF were seeded on triphasic tendon gels a 50,000 cells/gel, and Sket.4U were seeded on biphasic muscle gels at 100,000 cells/gel.

On days 1, 3, 7 and 14, DNA content (Figure 7A) and metabolic activity (Figure 7B) were assessed. MG-63 showed a decrease in DNA content over time, however, the metabolic activity increased over 7 days and then decreased insignificantly until day 14, indicating that fewer cells were more metabolically active. For HDF the DNA content increased at day 3 then it remained stable over 14 days. The metabolic activity increased until day 7, followed by a decrease on day 14. Sket.4U's DNA content remained consistent over 3 days. It then decreased significantly until day 14, while the metabolic activity increased until day 7, but then started to decrease again.

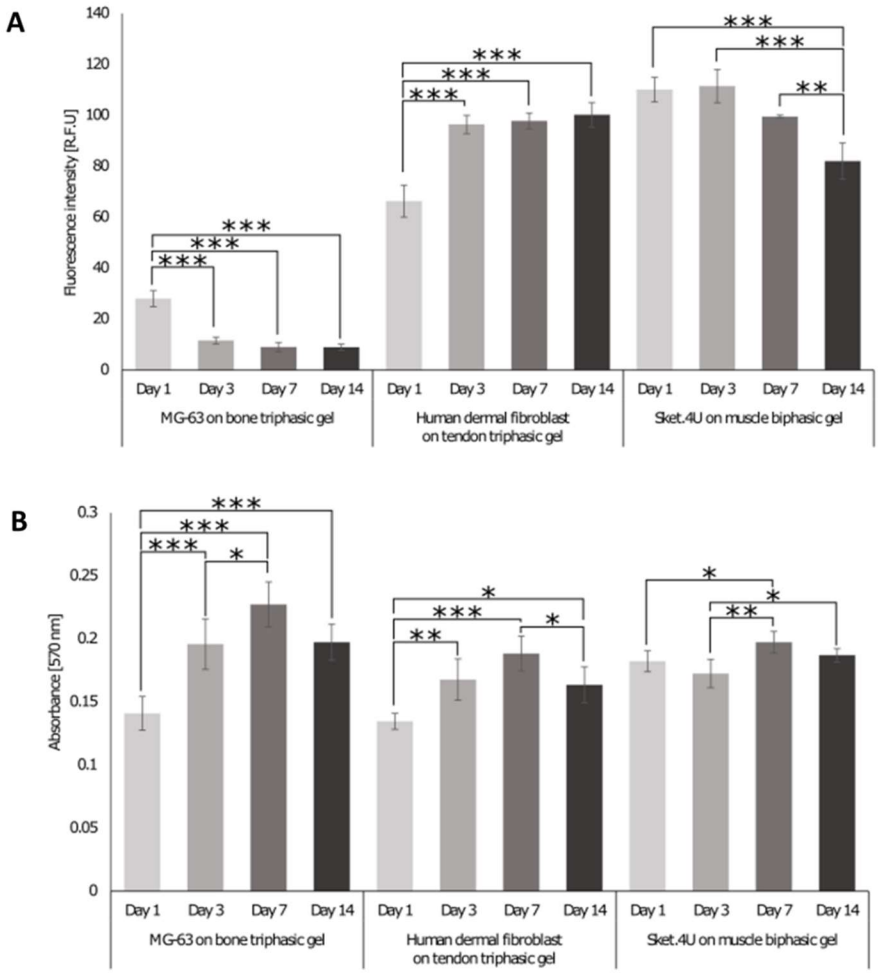

Figure 7. DNA content and metabolic activity assessed for cells seeded on triphasic and biphasic gels. MG-63 and human dermal fibroblast (HDF) were seeded with a seeding density of 50,000 cells/gel on the bone and tendon triphasic gels, respectively. Sket.4U were seeded on biphasic gels with a seeding density of 100,000 cells/gel. After 1,3,7 and 14 days from seeding A) DNA content was determined. Fluorescence intensity was read at excitation 480 nm, emission 520 nm. B) metabolic activity was assessed, and the absorbance was read at 570 nm and 600 nm. The experiment was performed in triplicate and three readings were done per sample (n=9). One-way ANOVA and Tukey post hoc test were performed, *=p<0.05, **=p<0.01, ***=p<0.001. Error bars show standard deviation.

3.5. Biological response of cells seeded on the 3D interface model

3.5.1. Comparison of growth chamber versus standard cell culture plate

To assess whether the chamber allows for cell growth and co-culture, the cell DNA content, metabolic activity, and cytotoxicity were assessed with PicoGreen, Alamar Blue (Figure 8) and Lactate dehydrogenase (LDH) cytotoxicity assay (Figure 9), respectively. Analysis was conducted over 14 days and results were compared with the cells' response seeded on the 3D model cultured in a standard 6-well plate where the different cell culture media were mixed at a ratio of 4ml:3ml:3ml for MG-63, HDF and Sket.4U respectively. The DNA content of cells decreased over 14 days for both culture formats (Figure 8A). On day 14, the DNA content of cells was lower for cells cultured in the growth chamber though the cell metabolic activity increased (Figure 8B). On day 14, the metabolic activity of cells in the growth chamber was higher than the cells in the well plate, meaning that the cells were more active even if the DNA content was lower.

When the cells were cultured in the 6-well plate, a decrease in the level of LDH occurred (Figure 9). In the growth chamber, LDH levels first decreased (day 7) and then increased until day 14. Data normalised to day 1 showed that the variation was lower for the growth chamber, as the values were 0.82 (day 7) and 0.92 (day 14); while for the well plate LDH were 0.89 (day 7) and 0.7 (day 14). However, on the final time point, the LDH released by the cells in the growth chamber was lower than the plate suggesting the growth camber was suitable to keep cells alive and active, with reduced levels of cytotoxicity. The higher metabolic activity of cells in the growth chamber compared to the 6-well plate may be due to the separation of the cell culture media. This method was therefore chosen to evaluate the cell response and interfaces formation over 21 days.

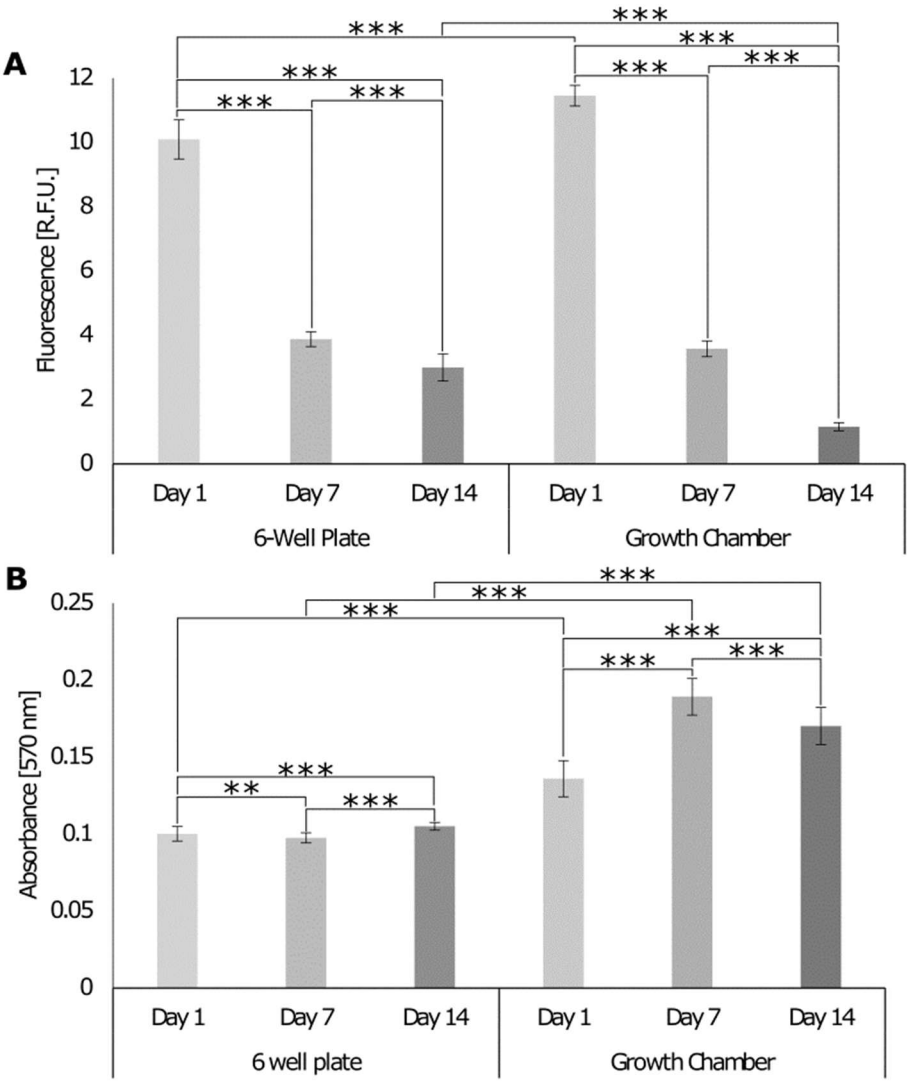

Figure 8. DNA content and metabolic activity of cells seeded on 3D models with topography cultured in 6-well plate or growth chamber. A) DNA content was assessed with PicoGreen assay. Fluorescence intensity read at excitation 480 nm, emission 520 nm (n=24). B) Cell metabolic activity was assessed with Alamar Blue. Absorbance was read at 570 nm and 600 nm (n=36). Two-way ANOVA and Tukey post hoc test were performed *= $p<0.05$, **=$p<0.01$, ***=$p<0.001$. Error bars show standard deviation.

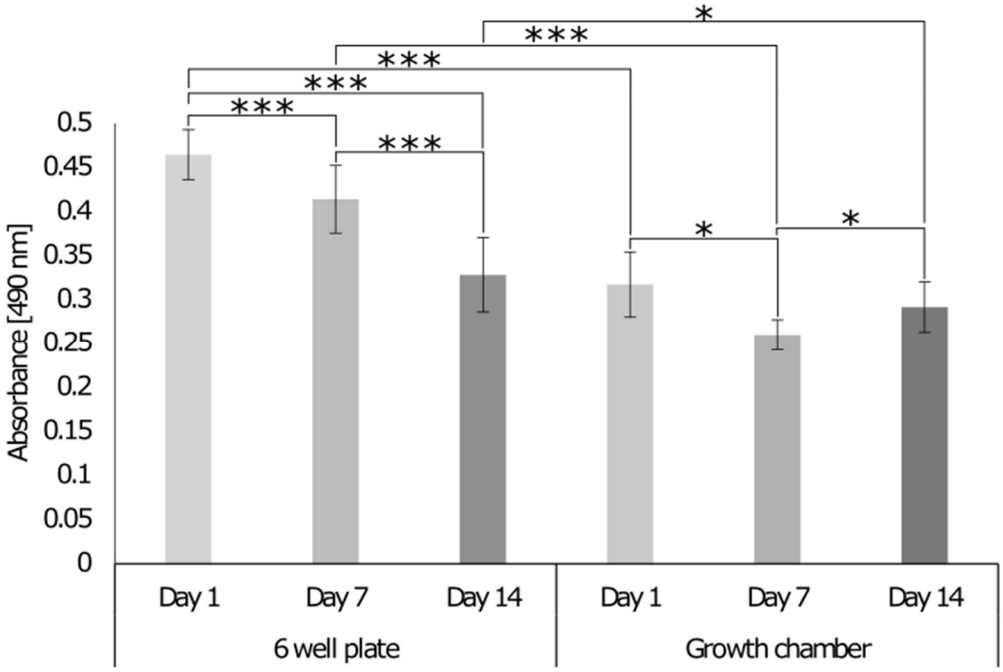

Figure 9. LDH release of cells seeded on 3D model cultured in 6-well plate or growth chamber. On day 1, 7 and 14 release of LDH was detected with LDH Cytotoxicity Assay. Absorbance was read at 490 nm and 680 nm. Two-way ANOVA and Tukey post hoc test were performed *= $p<0.05$, **=$p<0.01$, ***=$p<0.001$. Error bars show standard deviation (n=9).

3.5.2 Biological response of cells cultures on the 3D in vitro interface model

When cells were cultured on the 3D *in vitro* model in the growth chamber, the DNA content decreased until day 14 and then stabilized at day 21 (Figure 10A). The cells' metabolic activity increased until day 7 and decreased by day 14, while it stabilized at day 21 (**Error! Reference source not found.**10B), indicating that cells were still metabolically active and reached homeostasis at day 14. On day 1, various dead cells in the bone and muscle area were observed (Figure 11), but in general, the number of live cells was higher than the number of dead cells. On day 7, fewer dead cells were detected in all sections and the brightness of living cells increased, suggesting an increase in metabolic activity. Subsequently, the brightness decreased again, and more dead cells were visible on day 14 and day 21. Data were confirmed with LDH cytotoxicity assay which showed that LDH release decreased on day 7 and increased on day 14 to remain stable at day 21 (Figure 12).

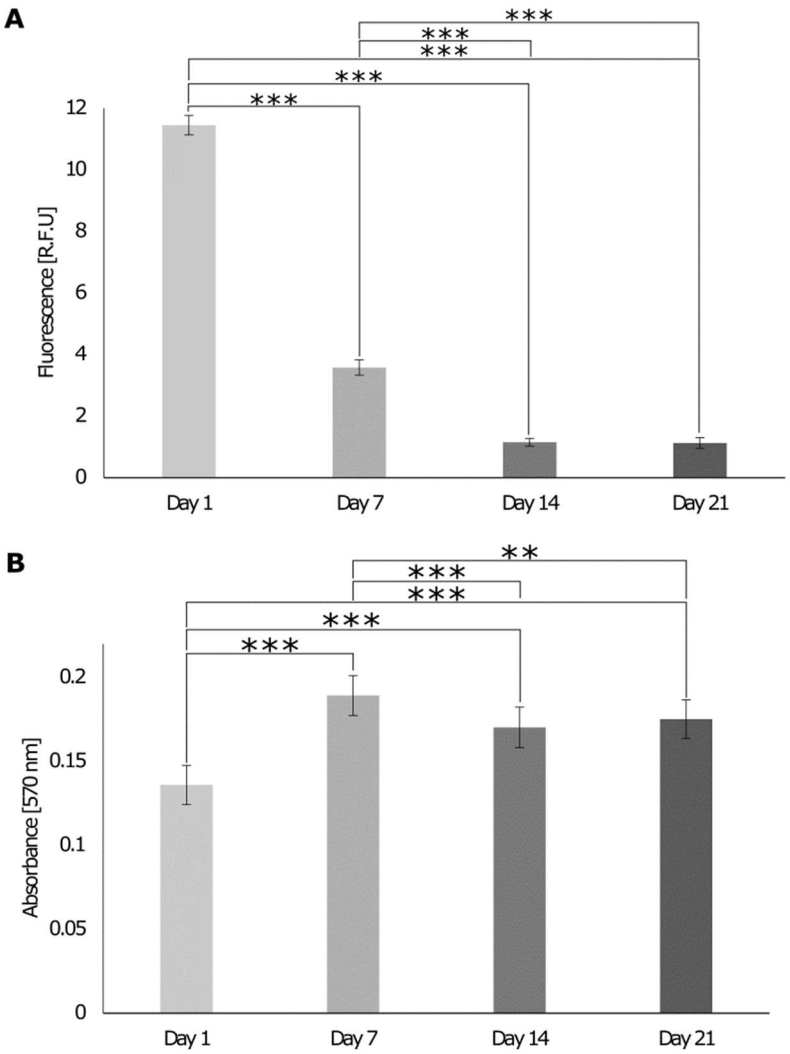

Figure 10. Evaluation of DNA content and cell metabolic activity of cells seeded on 3D interface model in growth chamber over 21 days. On day 1, 7, 14 and 21 A) DNA content was assessed with PicoGreen assay. Fluorescence intensity read at excitation 480 nm, emission 520 nm (n=24). B) Cell metabolic activity was assessed with Alamar blue. Absorbance was read at 570 nm and 600 nm. One-way ANOVA and Tukey post hoc test were performed *= $p<0.05$, **=$p<0.01$, ***=$p<0.001$. Error bars show standard deviation (n=36).

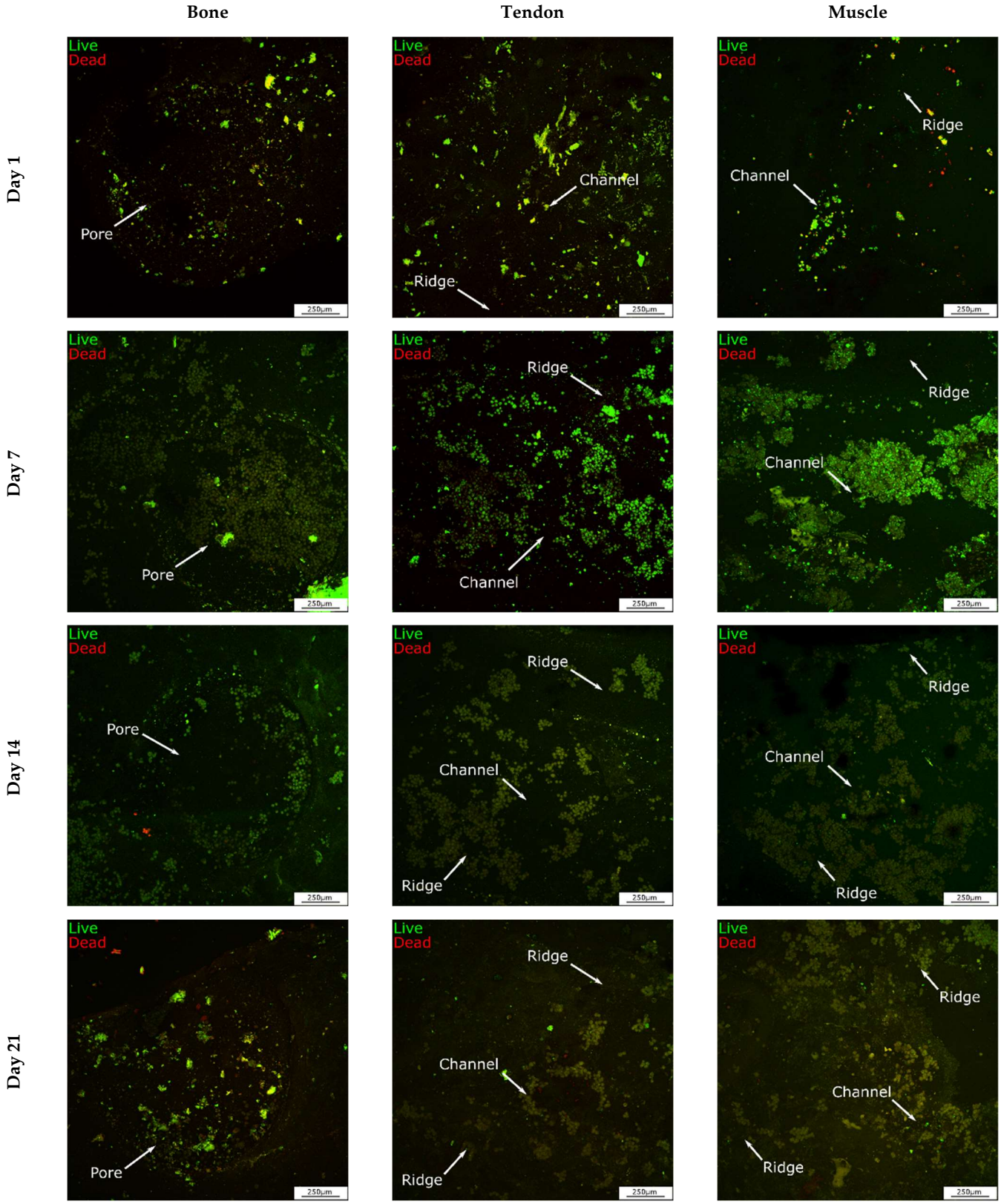

Figure 11. Viability of cells seeded on the 3D interface model cultured in the growth chamber over 21 days. On day 1, 7, 14, and 21 cells were stained with Live/Dead™. Cells were imaged with confocal microscope with 10x magnification. Live cells are stained in green, dead cells are stained in red. Scale bar = 250 µm.

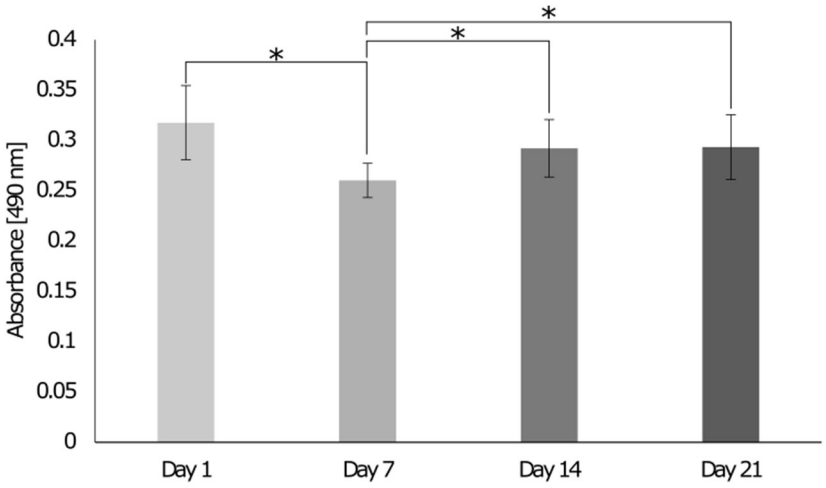

Figure 12. Evaluation of LDH release of cells seeded on the 3D interface model cultured in the growth chamber over 21 days. On day 1, 7, 14 and 21 LDH release was detected with LDH Cytotoxicity Assay. Absorbance was read at 490 nm and 680 nm. One-way ANOVA and Tukey post hoc test were performed *= p<0.05, **=p<0.01, ***=p<0.001. Error bars show standard deviation (n=9).

3.5.3 Assessment of tissue interface development

To identify the cell types, present in all sections of the 3D *in vitro* model, the expression of tissue-specific markers was assessed by immunocytochemistry and cells were imaged with a confocal microscope (Figure 13). On day 1, MG-63 expressed osteonectin, HDF expressed tenomodulin, and Sket.4U expressed αSMA. At the bone-tendon interface, both osteonectin and tenomodulin were expressed, while at the tendon-muscle interface both tenomodulin and αSMA were expressed. By day 14, cell numbers had decreased as indicated by the decrease in fluorescent signal. However, osteonectin tenomodulin, and αSMA were still expressed. At the bone-tendon interface mainly osteonectin with a low presence of tenomodulin were expressed, while at the tendon-muscle interface a high presence of tenomodulin was observed.

Cell morphology and matrix deposition were assessed with different histology stains (Figure 14, 15). For comparison with native tissues, mouse joints were also sectioned and stained. Alizarin red stains of the native joint (Figure 14) showed that a higher presence of calcium deposits was found in the bone and the muscle. Haematoxylin and Eosin (H&E) showed that cells in the native bone tissue are rounded and randomly organised, while in the tendon and muscle cells are aligned (Figure 14). Like the native tissues, a higher presence of calcium deposits was observed in the bone and muscle areas of the interface model (day 14) after which all tissues presented the same colour intensity (Figure 15). The colour intensity for Alizarin Red and H&E stains increased over time for all tissues. Cells started to align in the channels of tendon and muscle areas, however, fibre formation was not observed, correspondingly, MG-63 did not aggregate to form bone nodules.

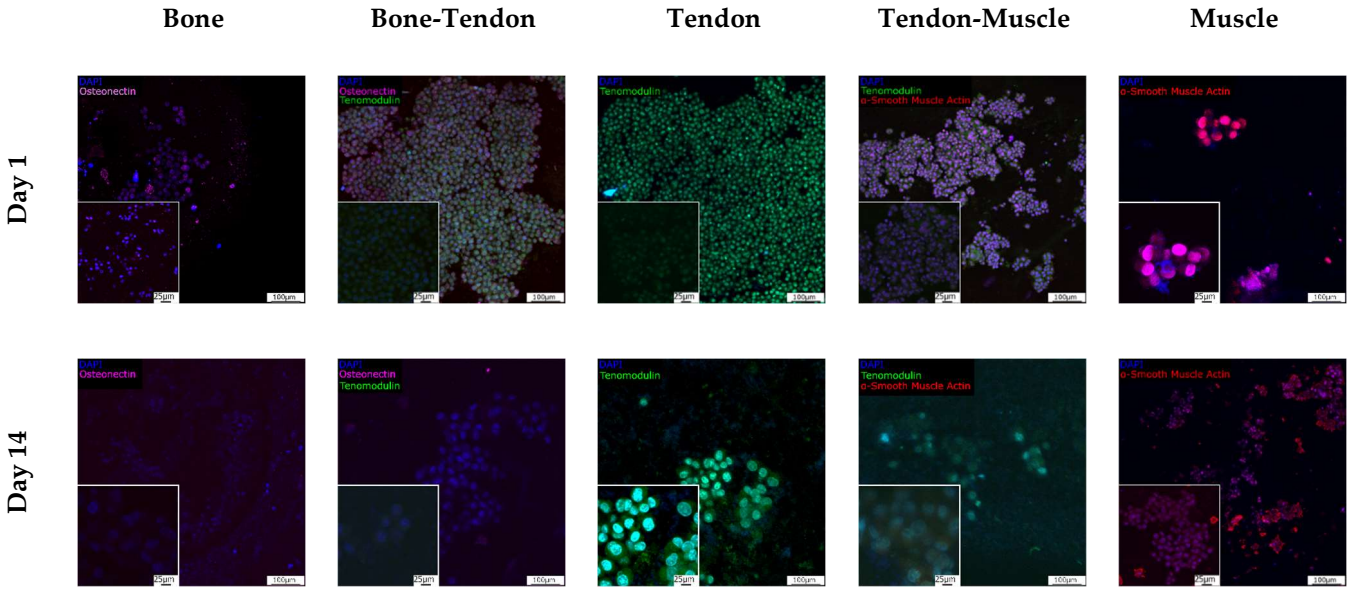

Figure 13. Expression of tissue-specific markers. Tissue-specific markers expression was assessed with immunocytochemistry. On day 1 and 14 cells were stained with osteonectin (magenta), tenomodulin (green) and αSMA (red). Nuclei were stained with DAPI (blue). Cells were imaged with a confocal microscope. Scale bars are 100 µm for 10x magnification and 25 µm for 40x magnification.

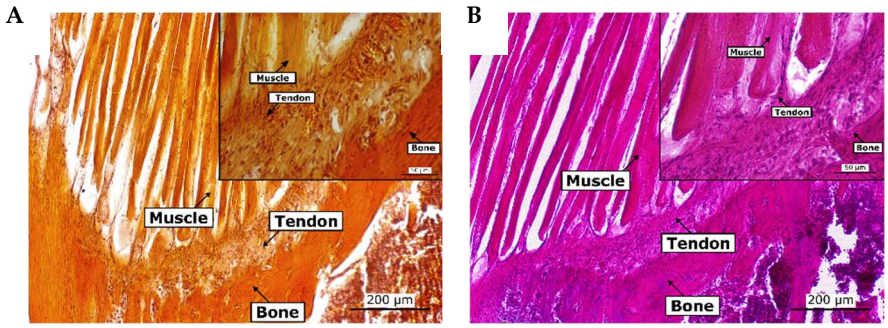

Figure 14. Histological stain of native tissue. Mouse joints were decalcified for 8 days and paraffin sections of 10 µm were prepared. Paraffin sections were stained with alizarin red (A) and haematoxylin and eosin (B). Scale bars are 200 µm for 10x magnification and 50 µm for 40x magnification.

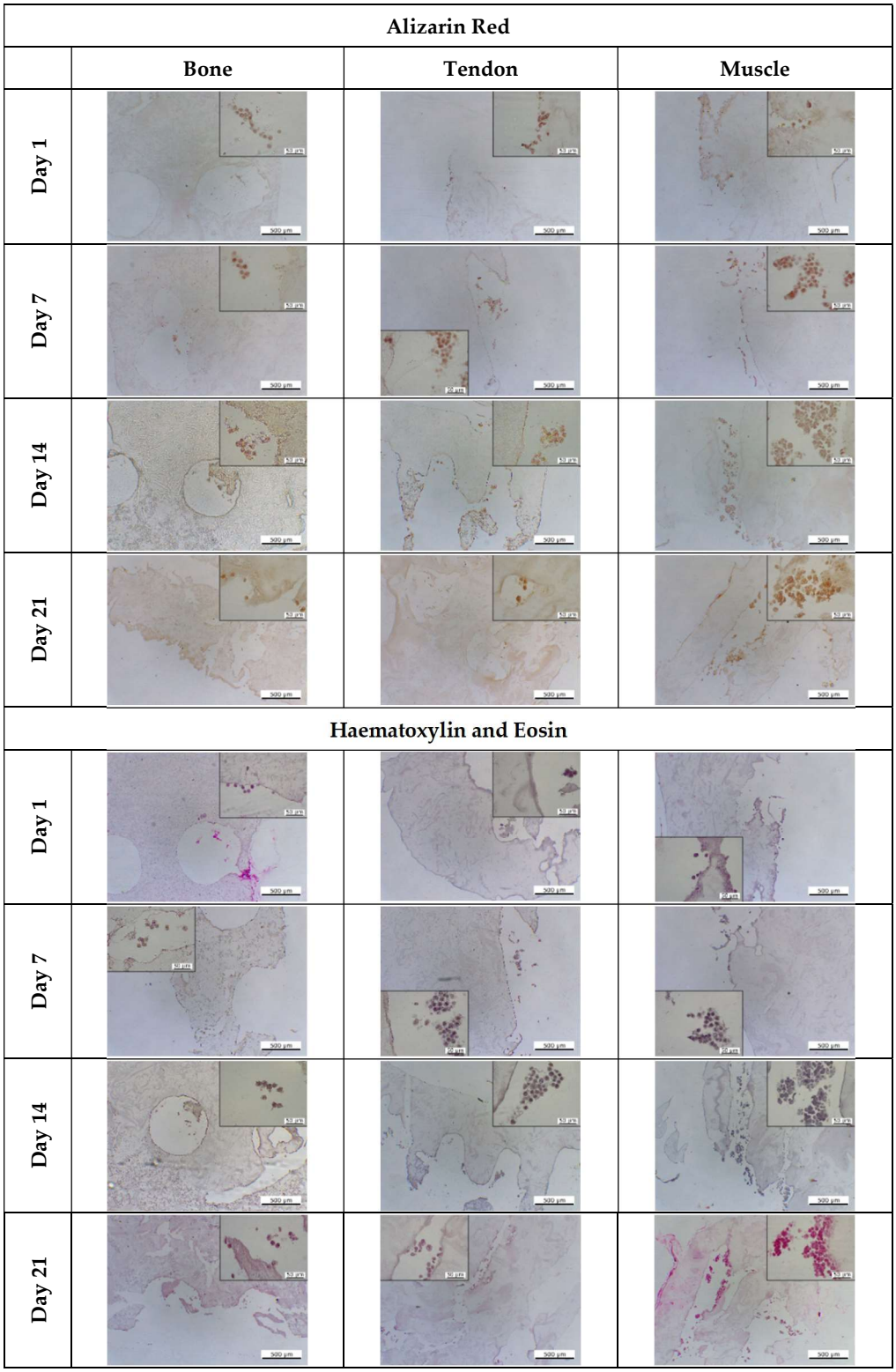

Figure 15. Histological assessment of the 3D interface model for matrix and calcium deposition. At day 1, 7, 14 and 21 the 3D model was sectioned and stained with alizarin red. Alizarin red stains calcium deposits in red/orange. Haematoxylin stains the nuclei purple, and eosin stains the cytoplasm pink. Scale bar are 500 µm for 4x magnification and 50 µm for 40x magnification.

4. Discussion

This study aimed to develop a 3D *in vitro* interface model by co-culturing of MG-63, HDF and Sket.4U in a newly developed growth chamber. When interfaces are studied, different tissues must be resembled. These tissues have different compositions, shapes, and physical properties, which can be mimicked in different layers. The layers can be joined with glues, sutures, or kitting, resulting often in uneven scaffolds [50–52]. To obtain scaffolds with a smooth, physiologically relevant transition between the phases, gradients in physical and chemical properties can be developed within the scaffold [14]. Synthetic polymers, like poly (lactic-co-glycolic acid) (PLGA) [5,15–17], poly (caprolactone) (PCL) [5,18–20] and poly (lactic acid) (PLA) [18,21–23] are commonly used because they are easy to handle but can be toxic and do not promote cell adhesion. Natural polymers, such as collagen, a protein present in bone [1], tendon [65], and muscle [11], are widely used in tissue engineering. Together with bone [30], tendon [31] and muscle [33]; collagen has been also used for nerve [66-69], cartilage [70-72] and skin [73-75] tissue engineering. Collagen was also used in breast cancer studies [76], [77]. To enhance its mechanical properties, it is commonly used with other materials [54–60], such as glycosaminoglycans and calcium phosphates to mimic bone and tendon [82]. Kim B et al. 2013 also used collagen to study the enthesis by mixing collagen with calcium phosphate in different concertation to mimic the different areas of the enthesis[39].

In this study, the 3D *in vitro* model was composed of three sections with tissue-specific surface topographies (**Error! Reference source not found.**A-B). The 3D *in vitro* interface model was fabricated by indirect 3D printing using a vertical mould with the negative shape of the model. Using indirect 3D printing it was possible to obtain a 3D *in vitro* model with complex shape, made from natural polymers [83]. A stiffness gradient was successfully developed by adding different concentrations of hydroxyapatite, namely 40% (v/v) for bone, 0.2% (v/v) for tendon, and 0% (v/v) for muscle (**Error! Reference source not found.**C). The concentrations were chosen aiming to resemble the inorganic phase of the tissues. In fact, in the native bone, the inorganic phase represents 40% of the total volume [84], while for the native tendon it is 0.2% [9], and the native muscle extracellular matrix (ECM) does not comprehend inorganic components [11].

The Young's modulus of biphasic muscle gel was about 20 kPa. In a healthy human body, the muscle's elastic moduli range from about 26 kPa (quadriceps, male, 22 years old) [69] to about 237 kPa (supraspinatus, male and female, 50 years old) [70]. The Young's modulus of triphasic tendon gel was about 140 kPa. Tendon's elastic moduli vary from around 8 kPa (Achilles' tendon, female 40 years old) [67] to about 4.5×10^5 kPa (tibialis anterior tendon, male, 22 years old) [68]. Finally, the Young's modulus of triphasic bone gel was about 240 kPa. In the body, the range of Young's moduli for bone is between ~3×10^4 kPa (calcaneus, male and female, 23-67 years old) [65] and ~2.6×10^7 kPa (femur, male and female, 53-93 years old) [66]. The Young's modulus of triphasic bone hydrogel was not in the range of native bone. To date, the maximum Young's modulus reached with crosslinked hydrogels is approximately 80 MPa [71]. Considering that the forces native tissues are subjected to are higher *in vivo* than *in vitro* [72,73], reaching Young's moduli of native tissues might not be essential to enhance cellular responses. Hence, the values obtained in this study were considered appropriate to resemble the interfaces, as there was an increase in stiffness from muscle to bone.

MG-63 were found suitable to resemble bone as they expressed osteonectin and organised in aggregates reflecting bone nodules. HDF can be used as tenocyte models as they started to align in the same direction and expressed tenomodulin. Sket.4U expressed αSMA and aligned along the gels in the same directions though no fibre formation was observed. We hypothesized that it might require a higher cell number or a longer culture time to show organization in fibres. Nevertheless, Sket.4U were found suitable to mimic skeletal myoblasts. Cell seeding densities that allowed cells to reach homeostasis

individually on biphasic were determined. Homeostasis is a "self-regulating process by which biological systems maintain stability while adjusting to changing external conditions" [85]. When cells reach homeostasis, they cease proliferation and migration and instead begin differentiation or new matrix production eventually forming tissue interfaces [86]. We found that 50,000 cells/gel for MG-63 and HDF, and 100,000 cells/ gel for Sket.4U allowed cells to reach homeostasis (Figure 6).

When seeded on the bone triphasic hydrogel, MG-63's DNA content decreased until day 7, but then remained constant until day 14. The cell metabolic activity increased until day 7 and remained stable until day 14. DNA content has been related to cell number, because in cells the overall level of nucleic acids is constant and strongly regulated, even if the levels of DNA or RNA can vary [76, 77]. Therefore, a decrease in DNA content is linked to a decrease in cell number. This means that the cells were metabolically active, even if the cell number did not increase. For these reasons, the bone triphasic hydrogel was found appropriate for cell culture.

HDF on triphasic tendon hydrogel reached homeostasis after 7 days indicated by the stable DNA content between day 7 and day 14. Their metabolic activity increased until day 7 and decreased on day 14. Sket.4U on the biphasic hydrogels did not show significant changes in DNA content until day 14. The metabolic activity increased on day 7 and remained stable until day 14. Consequently, the tendon triphasic and the muscle biphasic hydrogels were found suitable for cell culture.

In tissue interface studies different tissues are investigated simultaneously, requiring advanced co-culture approaches. When different cells are seeded on the same substrate (direct co-culture), it is essential to keep under consideration that different cell types may require different cell media, as these might have distinct functions. One of the approaches involves mixing different media in different ratios, but supplements can affect the other cell types [89]. Instead, supplements appropriate for all cell types can be added to a basal medium [21, 25]. Nevertheless, medium optimisation can be time-consuming and costly [54]. Otherwise, a device that keeps the different media physically separated while cell-cell contact is allowed can be developed [90]. This method was examined in this study, where a growth chamber was developed for this purpose. The chamber was made of three compartments, one for each tissue, separated by partial walls that avoided the mixing of media, but allowing the insertion of the 3D *in vitro* model, and cell-cell communication (**Error! Reference source not found.**).

Testing the mixing of liquids within the chamber, revealed that after 24 hours, limited mixing of the liquids occurred. The mixing was marginal and acceptable, as in the body tissues are not completely isolated and gradually change in chemical composition [91]. Clear resin was easy to sterilise and prevented cell adhesion on its own. This should enhance cell adhesion to the 3D *in vitro* interface model, being the only biologically suitable substrate for cell growth. The chamber was designed to allow the connection to a peristaltic pump to provide a dynamic medium flow to cells, improving the gas and nutrient circulation and enhancing cell proliferation and migration [81–86]. Nevertheless, the cell response in dynamic conditions was not assessed in this study. A comparison of the results obtained in dynamic conditions with the ones obtained in this study would be of great interest. Cell culture studies for tissue engineering purposes frequently have too short culture times to accurately imitate tissue regeneration processes *in vitro* [25,47–49]. Studies that are conducted over shorter time frames cannot sufficiently determine whether the method is appropriate since complete tissue repair and regeneration can take weeks to months [98]. Here, cells were cultured over 21 days. Results showed that cells on the 3D *in vitro* model reached homeostasis at day 14, however, the number of cells seeded was not high enough to allow the formation of relevant biological structures, such as bone nodules as well as tendon and muscle fibres. Cell DNA content decreased with time, but cells were metabolically active (Figure 10). Alizarin red and H&E stain confirmed that

cells deposited new matrix, which could explain the increase in metabolic activity (Figure 15).

In literature, cell phenotype and genotype at tissue interfaces are not always investigated [23, 44–46]. Here, the expression of tissue-specific markers was assessed in all the sections of the 3D *in vitro* model, namely bone, bone-tendon, tendon, tendon-muscle, and muscle (Figure 13). It was assumed that cells expressed tissue-specific markers relevant to the section of the *in vitro* model they were cultured in. However, the expression of osteonectin, tenomodulin and α-SMA decreased at day 14. Osteonectin was dominantly present at the bone-tendon interface and tenomodulin at the tendon-muscle interface. The low cell population at this time point may be the cause of the decreasing fluorescent signal. Higher cell seeding densities might be required so that cells can adjust to the transition from a standard 2D culture to the 3D *in vitro* model. Furthermore, even if osteonectin is widely expressed in mineralised tissues, fibroblast also stained positive for this marker [99]. Thus, the cells expressing osteonectin can be both MG-63 and HDF. Additionally, it is important to consider that MG-63 is an osteosarcoma cell line. In another study, when MG-63 were co-cultured with fibroblast, they increased their migration towards the direction of fibroblast [100]. Thus, the high presence of osteonectin at the interface could be explained by a higher presence of MG-63 compared to HDF. Similarly, fibroblasts are known to be migrating [101], suggesting they may have migrated to the tendon-muscle interface. Furthermore, when seeded in 2D, MG-63 showed higher metabolic activity than the other cell types; while Sket.4U were less active (supplementary data, Figure S1). This can be another reason why osteonectin and tenomodulin were more expressed at the interfaces. Finally, in this study cells were seeded simultaneously. However, because these cell types showed different proliferation rates and metabolic activities, seeding them one at a time might allow establishing stable cell populations providing more time for less proliferative cells to reach homeostasis. Hence, Sket.4U should be seeded first, followed by HDF and MG-63. It could be interesting to test bone, tendon, and muscle primary cells' response to assess whether this 3D *in vitro* model could be customized with cells from a patient to regenerate tissue interfaces. Also, assessing if the construct can promote mesenchymal stem cell differentiation into bone, tendon, and muscle cells could be of great interest.

5. Conclusion

A 3D *in vitro* model of bone-tendon-muscle interface was developed and validated. It was type I collagen/agarose based, with a gradient in hydroxyapatite, decreasing from bone to muscle. MG-63, HDF, and Sket.4U cells were co-cultured over 21 days. Studies were conducted in a growth chamber that allowed cell culture media to remain separated while allowing cell communication. Cells expressed tissue-specific markers and produced new matrix. The 3D *in vitro* interface model facilitated the increase in cell numbers and metabolic activities and could potentially allow the formation of tissue interfaces. Applications for this 3D *in vitro* model include studies of disorders, cancer, or ageing on the interface, as well as drug discovery and drug testing. Furthermore, this new 3D *in vitro* model could be used for the regeneration of the interfaces in patients who have experienced injuries or degeneration.

Author Contributions: Conceptualization, W.B. and Y.R.; Methodology, W.B., G.H.; Validation, W.B., R.M., J.H. and Y.R.; Formal Analysis, W.B.; Investigation, W.B., G.H.; Resources, Y.R.; Data Curation, W.B.; Writing – Original Draft Preparation, W.B.; Writing – Review & Editing, Y.R., J.H. and R.M; Visualization, W.B., G.H.; Project Administration, W.B.; Funding Acquisition and Supervision, Y.R.

Acknowledgments: The authors would like to thank Nottingham Trent University and MechAscan (EP/P031137/1) for funding this project. We also thank Dominic Craske and Gareth Williams for their help with scanning electron microscope and histology.

Conflicts of Interest: The authors declare no conflicts of interest

References

[1] P. J. Yang and J. S. Temenoff, "Engineering Orthopedic Tissue Interfaces," *Tissue Eng Part B Rev*, vol. 15, no. 2, pp. 127–141, 2009, doi: 10.1089/ten.teb.2008.0371.

[2] H. H. Lu, S. D. Subramony, M. K. Boushell, and X. Zhang, "Tissue engineering strategies for the regeneration of orthopedic interfaces," *Ann Biomed Eng*, vol. 38, no. 6, pp. 2142–2154, Jun. 2010, doi: 10.1007/s10439-010-0046-y.

[3] O. O. Babatunde, J. L. Jordan, D. A. van der Windt, J. C. Hill, N. E. Foster, and J. Protheroe, "Effective treatment options for musculoskeletal pain in primary care: A systematic overview of current evidence," *PLoS ONE*, vol. 12, no. 6. Public Library of Science, 2017. doi: 10.1371/journal.pone.0178621.

[4] W. Balestri, R. Morris, J. Hunt, and Y. Reinwald, "Current advances on the regeneration of musculoskeletal interfaces," *Tissue Eng Part B Rev*, Nov. 2020, doi: 10.1089/ten.teb.2020.0112.

[5] W. Liu, J. Lipner, J. Xie, C. N. Manning, S. Thomopoulos, and Y. Xia, "Nanofiber scaffolds with gradients in mineral content for spatial control of osteogenesis," *ACS Appl Mater Interfaces*, vol. 6, no. 4, pp. 2842–2849, Feb. 2014, doi: 10.1021/AM405418G/SUPPL_FILE/AM405418G_SI_001.PDF.

[6] W. J. Landis, K. J. Hodgens, J. Arena, M. J. Song, and B. F. McEwen, "Structural relations between collagen and mineral in bone as determined by high voltage electron microscopic tomography," *Microscopy Research and Technique*, vol. 33, no. 2. John Wiley & Sons, Ltd, pp. 192–202, Feb. 01, 1996. doi: 10.1002/(SICI)1097-0029(19960201)33:2<192::AID-JEMT9>3.0.CO;2-V.

[7] L. Baldino, S. Cardea, N. Maffulli, and E. Reverchon, "Regeneration techniques for bone-To-Tendon and muscle-To-Tendon interfaces reconstruction," *Br Med Bull*, vol. 117, no. 1, pp. 25–37, 2016, doi: 10.1093/bmb/ldv056.

[8] Y. Xiong, H. J. Yang, J. Feng, Z. L. Shi, and L. D. Wu, "Effects of alendronate on the proliferation and osteogenic differentiation of MG-63 cells," *Journal of International Medical Research*, vol. 37, no. 2, pp. 407–416, Mar. 2009, doi: 10.1177/147323000903700216.

[9] F. Wu, M. Nerlich, and D. Docheva, "Tendon injuries: Basic science and new repair proposals," *EFORT Open Rev*, vol. 2, no. 7, pp. 332–342, Jul. 2017, doi: 10.1302/2058-5241.2.160075.

[10] T. H. Qazi, D. J. Mooney, M. Pumberger, S. Geißler, and G. N. Duda, "Biomaterials based strategies for skeletal muscle tissue engineering: Existing technologies and future trends," *Biomaterials*, vol. 53, pp. 502–521, 2015, doi: 10.1016/j.biomaterials.2015.02.110.

[11] A. R. Gillies and R. L. Lieber, "Structure and function of the skeletal muscle extracellular matrix," *Muscle Nerve*, vol. 44, no. 3, pp. 318–331, Sep. 2011, doi: 10.1002/mus.22094.

[12] E. Bayrak and P. Yilgor Huri, "Engineering musculoskeletal tissue interfaces," *Frontiers in Materials*, vol. 5. Frontiers Media S.A., p. 24, Apr. 30, 2018. doi: 10.3389/fmats.2018.00024.

[13] W. J. King and P. H. Krebsbach, "Multi-Tissue Interface Bioengineering," in *Stem Cell Biology and Tissue Engineering in Dental Sciences*, Elsevier Inc., 2015, pp. 593–602. doi: 10.1016/B978-0-12-397157-9.00048-5.

[14] C. Pitta Kruize *et al.*, "Biomimetic Approaches for the Design and Fabrication of Bone-to-Soft Tissue Interfaces," *ACS Biomater Sci Eng*, 2021, doi: 10.1021/ACSBIOMATERIALS.1C00620/ASSET/IMAGES/ACSBIOMATERIALS.1C00620.SOCIAL.JPEG_V03.

[15] C. Z. Mosher, J. P. Spalazzi, and H. H. Lu, "Stratified scaffold design for engineering composite tissues," *Methods*, vol. 84, pp. 99–102, Aug. 2015, doi: 10.1016/J.YMETH.2015.03.029.

[16] J. Lipner *et al.*, "The mechanics of PLGA nanofiber scaffolds with biomimetic gradients in mineral for tendon-to-bone repair," *J Mech Behav Biomed Mater*, vol. 40, pp. 59–68, Dec. 2014, doi: 10.1016/j.jmbbm.2014.08.002.

[17] H. H. Lu *et al.*, "Anterior cruciate ligament regeneration using braided biodegradable scaffolds: In vitro optimization studies," *Biomaterials*, vol. 26, no. 23, pp. 4805–4816, 2005, doi: 10.1016/j.biomaterials.2004.11.050.

[18] T. Baudequin *et al.*, "The osteogenic and tenogenic differentiation potential of C3H10T1/2 (mesenchymal stem cell model) cultured on PCL/PLA electrospun scaffolds in the absence of specific differentiation medium," *Materials*, vol. 10, no. 12, pp. 1–19, 2017, doi: 10.3390/ma10121387.

[19] F. Han, P. Zhang, Y. Sun, C. Lin, P. Zhao, and J. Chen, "Hydroxyapatite-doped polycaprolactone nanofiber membrane improves tendon–bone interface healing for anterior cruciate ligament reconstruction," *Int J Nanomedicine*, vol. 10, pp. 7333–7343, 2015, doi: 10.2147/IJN.S92099.

[20] J. Nowlin, M. A. Bismi, B. Delpech, P. Dumas, Y. Zhou, and G. Z. Tan, "Engineering the hard-soft tissue interface with random-to-aligned nanofiber scaffolds.," *Nanobiomedicine (Rij)*, vol. 5, p. 1849543518803538, Oct. 2018, doi: 10.1177/1849543518803538.

[21] J. O. Cooper, J. D. Bumgardner, J. A. Cole, R. A. Smith, and W. O. Haggard, "Co-cultured tissue-specific scaffolds for tendon/bone interface engineering," *J Tissue Eng*, vol. 5, no. X, p. 204173141454229, 2014, doi: 10.1177/2041731414542294.

[22] J. Guo, W. Su, J. Jiang, C. Ning, J. Zhao, and X. Liu, "Enhanced tendon to bone healing in rotator cuff tear by PLLA/CPS composite films prepared by a simple melt-pressing method: An in vitro and in vivo study," *Compos B Eng*, vol. 165, pp. 526–536, May 2019, doi: 10.1016/j.compositesb.2019.02.003.

[23] S. K. Madhurakkat Perikamana *et al.*, "Harnessing biochemical and structural cues for tenogenic differentiation of adipose derived stem cells (ADSCs) and development of an in vitro tissue interface mimicking tendon-bone insertion graft," *Biomaterials*, vol. 165, pp. 79–93, 2018, doi: 10.1016/j.biomaterials.2018.02.046.

[24] P. v. Kolluru *et al.*, "Strong and tough mineralized PLGA nanofibers for tendon-to-bone scaffolds," *Acta Biomater*, vol. 9, no. 12, pp. 9442–9450, Dec. 2013, doi: 10.1016/J.ACTBIO.2013.07.042.

[25] T. K. Merceron *et al.*, "A 3D bioprinted complex structure for engineering the muscle-tendon unit," *Biofabrication*, vol. 7, no. 3, p. 35003, 2015, doi: 10.1088/1758-5090/7/3/035003.

[26] R. Schweitzer *et al.*, "Analysis of the tendon cell fate using Scleraxis, a specific marker for tendons and ligaments," *Development*, vol. 128, no. 19, pp. 3855–3866, 2001.

[27] F. J. O'Brien, "Biomaterials & scaffolds for tissue engineering," *Materials Today*, vol. 14, no. 3. Elsevier B.V., pp. 88–95, Mar. 01, 2011. doi: 10.1016/S1369-7021(11)70058-X.

[28] A. Domingues Goncalves, W. Balestri, and Y. Reinwald, "Biomedical Implants for Regenerative Therapies," in *Biomaterials [Working Title]*, IntechOpen, 2020. doi: 10.5772/intechopen.91295.

[29] S. Fu and P. Zhang, "Surface modification of polylactic acid (PLA) and polyglycolic acid (PGA) monofilaments via the cold plasma method for acupoint catgut-embedding therapy applications," *Textile Research Journal*, vol. 89, no. 18, pp. 3839–3849, Sep. 2019, doi: 10.1177/0040517518824841.

[30] Z. Yuan, K. Memarzadeh, A. S. Stephen, R. P. Allaker, R. A. Brown, and J. Huang, "Development of a 3D Collagen Model for the In Vitro Evaluation of Magnetic-assisted Osteogenesis," *Sci Rep*, vol. 8, no. 1, Dec. 2018, doi: 10.1038/s41598-018-33455-2.

[31] S. R. Caliari, M. A. Ramirez, and B. A. C. Harley, "The development of collagen-GAG scaffold-membrane composites for tendon tissue engineering," *Biomaterials*, vol. 32, no. 34, pp. 8990–8998, Dec. 2011, doi: 10.1016/j.biomaterials.2011.08.035.

[32] V. Farano *et al.*, "Bioactivity evaluation of collagen-based scaffolds containing a series of Sr-doped melt-quench derived phosphate-based glasses," *J Mater Sci Mater Med*, vol. 29, no. 7, p. 101, 2018, doi: 10.1007/s10856-018-6110-0.

[33] R. Shah, J. C. Knowles, N. P. Hunt, and M. P. Lewis, "Development of a novel smart scaffold for human skeletal muscle regeneration," *J Tissue Eng Regen Med*, vol. 10, no. 2, pp. 162–171, Feb. 2016, doi: 10.1002/term.1780.

[34] B. Marelli *et al.*, "Collagen-Reinforced Electrospun Silk Fibroin Tubular Construct as Small Calibre Vascular Graft," *Macromol Biosci*, vol. 12, no. 11, pp. 1566–1574, Nov. 2012, doi: 10.1002/mabi.201200195.

[35] M. Achilli, J. Lagueux, and D. Mantovani, "On the effects of UV-C and pH on the mechanical behavior, molecular conformation and cell viability of collagen-based scaffold for vascular tissue engineering," *Macromol Biosci*, vol. 10, no. 3, pp. 307–316, Mar. 2010, doi: 10.1002/mabi.200900248.

[36] S. Korpayev, G. Kaygusuz, M. Şen, K. Orhan, Ç. Oto, and A. Karakeçili, "Chitosan/collagen based biomimetic osteochondral tissue constructs: A growth factor-free approach," *Int J Biol Macromol*, vol. 156, pp. 681–690, Aug. 2020, doi: 10.1016/j.ijbiomac.2020.04.109.

[37] M. Köpf, D. F. Duarte Campos, A. Blaeser, K. S. Sen, and H. Fischer, "A tailored three-dimensionally printable agarose-collagen blend allows encapsulation, spreading, and attachment of human umbilical artery smooth muscle cells," *Biofabrication*, vol. 8, p. 25011, May 2016, doi: 10.1088/1758-5090/8/2/025011.

[38] T. A. Ulrich, A. Jain, K. Tanner, J. L. MacKay, and S. Kumar, "Probing cellular mechanobiology in three-dimensional culture with collagen-agarose matrices," *Biomaterials*, vol. 31, no. 7, pp. 1875–1884, Mar. 2010, doi: 10.1016/J.BIOMATERIALS.2009.10.047.

[39] B. S. Kim, E. J. Kim, J. S. Choi, J. H. Jeong, C. H. Jo, and Y. W. Cho, "Human collagen-based multilayer scaffolds for tendon-to-bone interface tissue engineering," *J Biomed Mater Res A*, vol. 102, no. 11, pp. 4044–4054, Nov. 2014, doi: 10.1002/JBM.A.35057.

[40] A. A. Al-Munajjed *et al.*, "Development of a biomimetic collagen-hydroxyapatite scaffold for bone tissue engineering using a SBF immersion technique," *J Biomed Mater Res B Appl Biomater*, vol. 90 B, no. 2, pp. 584–591, Aug. 2009, doi: 10.1002/jbm.b.31320.

[41] L. Liu, L. Zhang, B. Ren, F. Wang, and Q. Zhang, "Preparation and Characterization of Collagen-Hydroxyapatite Composite Used for Bone Tissue Engineering Scaffold," *Artif Cells Blood Substit Immobil Biotechnol*, vol. 31, no. 4, pp. 435–448, 2003, doi: 10.1081/BIO-120025414.

[42] S. C. Rodrigues, C. L. Salgado, A. Sahu, M. P. Garcia, M. H. Fernandes, and F. J. Monteiro, "Preparation and characterization of collagen-nanohydroxyapatite biocomposite scaffolds by cryogelation method for bone tissue engineering applications," *J Biomed Mater Res A*, vol. 101 A, no. 4, pp. 1080–1094, Apr. 2013, doi: 10.1002/jbm.a.34394.

[43] A. M. Ross, Z. Jiang, M. Bastmeyer, and J. Lahann, "Physical Aspects of Cell Culture Substrates: Topography, Roughness, and Elasticity," *Small*, vol. 8, no. 3, pp. 336–355, Feb. 2012, doi: 10.1002/SMLL.201100934.

[44] I. A. Janson and A. J. Putnam, "Extracellular matrix elasticity and topography: Material-based cues that affect cell function via conserved mechanisms," *J Biomed Mater Res A*, vol. 103, no. 3, pp. 1246–1258, Mar. 2015, doi: 10.1002/JBM.A.35254.

[45] C. J. Bettinger, R. Langer, and J. T. Borenstein, "Engineering Substrate Topography at the Micro- and Nanoscale to Control Cell Function," *Angewandte Chemie International Edition*, vol. 48, no. 30, pp. 5406–5415, Jul. 2009, doi: 10.1002/ANIE.200805179.

[46] M. J. Dalby *et al.*, "The control of human mesenchymal cell differentiation using nanoscale symmetry and disorder," *Nature Materials 2007 6:12*, vol. 6, no. 12, pp. 997–1003, Sep. 2007, doi: 10.1038/nmat2013.

[47] H. J. Choi *et al.*, "MG-63 cells proliferation following various types of mechanical stimulation on cells by auxetic hybrid scaffolds," *Biomater Res*, vol. 20, no. 1, pp. 1–8, Nov. 2016, doi: 10.1186/S40824-016-0079-X/FIGURES/9.

[48] L. Shor, S. Güçeri, X. Wen, M. Gandhi, and W. Sun, "Fabrication of three-dimensional polycaprolactone/hydroxyapatite tissue scaffolds and osteoblast-scaffold interactions in vitro," *Biomaterials*, vol. 28, no. 35, pp. 5291–5297, Dec. 2007, doi: 10.1016/J.BIOMATERIALS.2007.08.018.

[49] W. S. Leong, S. C. Wu, K. W. Ng, and L. P. Tan, "Electrospun 3D multi-scale fibrous scaffold for enhanced human dermal fibroblast infiltration," *Int J Bioprint*, vol. 2, no. 1, pp. 81–92, Jan. 2016, doi: 10.18063/IJB.2016.01.002.

[50] Y. Wu, Z. Wang, J. Ying Hsi Fuh, Y. San Wong, W. Wang, and E. San Thian, "Direct E-jet printing of three-dimensional fibrous scaffold for tendon tissue engineering," *J Biomed Mater Res B Appl Biomater*, vol. 105, no. 3, pp. 616–627, Apr. 2017, doi: 10.1002/JBM.B.33580.

[51] S. Chen, T. Nakamoto, N. Kawazoe, and G. Chen, "Engineering multi-layered skeletal muscle tissue by using 3D microgrooved collagen scaffolds," *Biomaterials*, vol. 73, pp. 23–31, Dec. 2015, doi: 10.1016/j.biomaterials.2015.09.010.

[52] S. H. Cha, H. J. Lee, and W. G. Koh, "Study of myoblast differentiation using multi-dimensional scaffolds consisting of nano and micropatterns," *Biomater Res*, vol. 21, no. 1, pp. 1–9, Jan. 2017, doi: 10.1186/S40824-016-0087-X/FIGURES/6.

[53] M. R. Ladd, S. Jin, J. D. Stitzel, A. Atala, and J. J. Yoo, "Co-electrospun dual scaffolding system with potential for muscle e tendon junction tissue engineering," *Biomaterials*, vol. 32, no. 6, pp. 1549–1559, 2011, doi: 10.1016/j.biomaterials.2010.10.038.

[54] M. A. M. Vis, K. Ito, and S. Hofmann, "Impact of Culture Medium on Cellular Interactions in in vitro Co-culture Systems," *Front Bioeng Biotechnol*, vol. 8, p. 911, Aug. 2020, doi: 10.3389/FBIOE.2020.00911/BIBTEX.

[55] E. Harris *et al.*, "Biofabrication of soft tissue templates for engineering the bone–ligament interface," *Biotechnol Bioeng*, vol. 114, no. 10, pp. 2400–2411, 2017, doi: 10.1002/bit.26362.

[56] C. H. Chang, F. H. Lin, C. C. Lin, C. H. Chou, and H. C. Liu, "Cartilage tissue engineering on the surface of a novel gelatin-calcium- phosphate biphasic scaffold in a double-chamber bioreactor," *J Biomed Mater Res B Appl Biomater*, vol. 71, no. 2, pp. 313–321, 2004, doi: 10.1002/jbm.b.30090.

[57] G. Criscenti *et al.*, "Triphasic scaffolds for the regeneration of the bone–ligament interface," *Biofabrication*, vol. 8, no. 1, p. 15009, 2016, doi: 10.1088/1758-5090/8/1/015009.

[58] M. Su *et al.*, "Preparation of Decellularized Triphasic Hierarchical Bone-Fibrocartilage-Tendon Composite Extracellular Matrix for Enthesis Regeneration," *Adv Healthc Mater*, vol. 8, no. 19, p. 1900831, Oct. 2019, doi: 10.1002/adhm.201900831.

[59] K. L. Moffat, A. S.-P. Kwei, J. P. Spalazzi, S. B. Doty, W. N. Levine, and H. H. Lu, "Novel Nanofiber-Based Scaffold for Rotator Cuff Repair and Augmentation," *Tissue Eng Part A*, vol. 15, no. 1, pp. 115–126, 2009, doi: 10.1089/ten.tea.2008.0014.

[60] R. Scaffaro, F. Lopresti, L. Botta, S. Rigogliuso, and G. Ghersi, "Preparation of three-layered porous PLA/PEG scaffold: Relationship between morphology, mechanical behavior and cell permeability," *J Mech Behav Biomed Mater*, vol. 54, pp. 8–20, 2016, doi: 10.1016/j.jmbbm.2015.08.033.

[61] J. A. Cooper, H. H. Lu, F. K. Ko, J. W. Freeman, and C. T. Laurencin, "Fiber-based tissue-engineered scaffold for ligament replacement: Design considerations and in vitro evaluation," *Biomaterials*, vol. 26, no. 13, pp. 1523–1532, 2005, doi: 10.1016/j.biomaterials.2004.05.014.

[62] I. Casanellas, A. García-Lizarribar, A. Lagunas, and J. Samitier, "Producing 3D biomimetic nanomaterials for musculoskeletal system regeneration," *Frontiers in Bioengineering and Biotechnology*, vol. 6, no. SEP. Frontiers Media S.A., p. 128, Sep. 20, 2018. doi: 10.3389/fbioe.2018.00128.

[63] L. M. Cross, A. Thakur, N. A. Jalili, M. Detamore, and A. K. Gaharwar, "Nanoengineered biomaterials for repair and regeneration of orthopedic tissue interfaces," *Acta Biomater*, vol. 42, pp. 2–17, Sep. 2016, doi: 10.1016/J.ACTBIO.2016.06.023.

[64] L. Rossetti *et al.*, "The microstructure and micromechanics of the tendon–bone insertion," *Nature Materials 2017 16:6*, vol. 16, no. 6, pp. 664–670, Feb. 2017, doi: 10.1038/nmat4863.

[65] C.-F. Liu, L. Aschbacher-Smith, N. J. Barthelery, N. Dyment, D. Butler, and C. Wylie, "What We Should Know Before Using Tissue Engineering Techniques to Repair Injured Tendons: A Developmental Biology Perspective," *Tissue Eng Part B Rev*, vol. 17, no. 3, pp. 165–176, Jun. 2011, doi: 10.1089/ten.teb.2010.0662.

[66] Y.-S. Lee and T. Livingston Arinzeh, "Electrospun Nanofibrous Materials for Neural Tissue Engineering," *Polymers (Basel)*, vol. 3, pp. 413–426, 2011, doi: 10.3390/polym3010413.

[67] T. Liu, J. D. Houle, J. Xu, B. P. Chan, and S. Y. Chew, "Nanofibrous Collagen Nerve Conduits for Spinal Cord Repair," *https://home.liebertpub.com/tea*, vol. 18, no. 9–10, pp. 1057–1066, Feb. 2012, doi: 10.1089/TEN.TEA.2011.0430.

[68] A. H. Boecker *et al.*, "Pre-differentiation of mesenchymal stromal cells in combination with a microstructured nerve guide supports peripheral nerve regeneration in the rat sciatic nerve," *Wiley Online Library*, vol. 43, no. 3, pp. 404–416, Feb. 2015, doi: 10.1111/ejn.13052.

[69] M. Jorfi, C. D'Avanzo, D. Y. Kim, and D. Irimia, "Three-Dimensional Models of the Human Brain Development and Diseases," *Adv Healthc Mater*, vol. 7, no. 1, Jan. 2018, doi: 10.1002/ADHM.201700723.

[70] D. J. Griffin *et al.*, "Mechanical characterization of matrix-induced autologous chondrocyte implantation (MACI®) grafts in an equine model at 53 weeks," *J Biomech*, vol. 48, no. 10, pp. 1944–1949, Jul. 2015, doi: 10.1016/J.JBIOMECH.2015.04.010.

[71] V. Muhonen *et al.*, "Articular cartilage repair with recombinant human type II collagen/polylactide scaffold in a preliminary porcine study," *Wiley Online Library*, vol. 34, no. 5, pp. 745–753, May 2016, doi: 10.1002/jor.23099.

[72] X. Zheng *et al.*, "Enhancement of chondrogenic differentiation of rabbit mesenchymal stem cells by oriented nanofiber yarn-collagen type I/hyaluronate hybrid," *Materials Science and Engineering C*, vol. 58, pp. 1071–1076, Jan. 2016, doi: 10.1016/J.MSEC.2015.07.066.

[73] L. Ma *et al.*, "Collagen/chitosan porous scaffolds with improved biostability for skin tissue engineering," *Biomaterials*, vol. 24, no. 26, pp. 4833–4841, 2003, doi: 10.1016/S0142-9612(03)00374-0.

[74] K. S. Rho *et al.*, "Electrospinning of collagen nanofibers: Effects on the behavior of normal human keratinocytes and early-stage wound healing," *Biomaterials*, vol. 27, no. 8, pp. 1452–1461, Mar. 2006, doi: 10.1016/J.BIOMATERIALS.2005.08.004.

[75] H. Niehues, J. A. Bouwstra, A. el Ghalbzouri, J. M. Brandner, P. L. J. M. Zeeuwen, and E. H. van den Bogaard, "3D skin models for 3R research: The potential of 3D reconstructed skin models to study skin barrier function," *Exp Dermatol*, vol. 27, no. 5, pp. 501–511, May 2018, doi: 10.1111/EXD.13531.

[76] J. Campbell, A. Husmann, R. Hume, C. W.- Biomaterials, and undefined 2017, "Development of three-dimensional collagen scaffolds with controlled architecture for cell migration studies using breast cancer cell lines," *Elsevier*, vol. 114, pp.34-43, January 2017, doi: 10.1016/j.biomaterials.2016.10.048

[77] J. Sapudom, L. Kalbitzer, X. Wu, S. Martin, K. K.- Biomaterials, and undefined 2019, "Fibril bending stiffness of 3D collagen matrices instructs spreading and clustering of invasive and non-invasive breast cancer cells," Elsevier, vol. 193, pp 47-57, February 2019, doi: 10.1016/j.biomaterials.2018.12.010

[78] G. Wei and P. X. Ma, "Structure and properties of nano-hydroxyapatite/polymer composite scaffolds for bone tissue engineering," *Biomaterials*, vol. 25, no. 19, pp. 4749–4757, Aug. 2004, doi: 10.1016/j.biomaterials.2003.12.005.

[79] A. D. Nocera, R. Comín, N. A. Salvatierra, and M. P. Cid, "Development of 3D printed fibrillar collagen scaffold for tissue engineering," *Biomed Microdevices*, vol. 20, no. 2, pp. 1–13, Feb. 2018, doi: 10.1007/s10544-018-0270-z.

[80] C. Fuoco, L. L. Petrilli, S. Cannata, and C. Gargioli, "Matrix scaffolding for stem cell guidance toward skeletal muscle tissue engineering," *J Orthop Surg Res*, vol. 11, no. 1, p. 1, Jul. 2016, doi: 10.1186/s13018-016-0421-y.

[81] S. Chen, T. Nakamoto, N. Kawazoe, and G. Chen, "Engineering multi-layered skeletal muscle tissue by using 3D microgrooved collagen scaffolds," *Biomaterials*, vol. 73, pp. 23–31, Dec. 2015, doi: 10.1016/j.biomaterials.2015.09.010.

[82] S. R. Caliari, M. A. Ramirez, and B. A. C. Harley, "The development of collagen-GAG scaffold-membrane composites for tendon tissue engineering," *Biomaterials*, vol. 32, no. 34, pp. 8990–8998, Dec. 2011, doi: 10.1016/j.biomaterials.2011.08.035.

[83] A. Houben, J. van Hoorick, J. van Erps, H. Thienpont, S. van Vlierberghe, and P. Dubruel, "Indirect Rapid Prototyping: Opening Up Unprecedented Opportunities in Scaffold Design and Applications," *Annals of Biomedical Engineering*, vol. 45, no. 1. pp. 58–83, 2017. doi: 10.1007/s10439-016-1610-x.

[84] X. Feng, "Chemical and Biochemical Basis of Cell-Bone Matrix Interaction in Health and Disease," *Curr Chem Biol*, vol. 3, no. 2, pp. 189–196, Apr. 2009, doi: 10.2174/187231309788166398.

[85] G. E. Billman, "Homeostasis: The Underappreciated and Far Too Often Ignored Central Organizing Principle of Physiology," *Front Physiol*, vol. 11, p. 200, Mar. 2020, doi: 10.3389/FPHYS.2020.00200/BIBTEX.

[86] A. Seidi, M. Ramalingam, I. Elloumi-Hannachi, S. Ostrovidov, and A. Khademhosseini, "Gradient biomaterials for soft-to-hard interface tissue engineering," 2011, doi: 10.1016/j.actbio.2011.01.011.

[87] O. S. Frankfurt, "Flow cytometric analysis of double-stranded RNA content distributions," *Journal of Histochemistry and Cytochemistry*, vol. 28, no. 7, pp. 663–669, Jan. 1980, doi: 10.1177/28.7.6156201.

[88] L. J. Jones, M. Gray, S. T. Yue, R. P. Haugland, and V. L. Singer, "Sensitive determination of cell number using the CyQUANT® cell proliferation assay," *J Immunol Methods*, vol. 254, no. 1–2, pp. 85–98, Aug. 2001, doi: 10.1016/S0022-1759(01)00404-5.

[89] F. Langenbach and J. Handschel, "Effects of dexamethasone, ascorbic acid and β-glycerophosphate on the osteogenic differentiation of stem cells in vitro," *Stem Cell Res Ther*, vol. 4, no. 5, pp. 1–7, Sep. 2013, doi: 10.1186/SCRT328/FIGURES/1.

[90] G. Robertson, T. J. Bushell, and M. Zagnoni, "Chemically induced synaptic activity between mixed primary hippocampal co-cultures in a microfluidic system," *Integrative Biology*, vol. 6, no. 6, pp. 636–644, Jun. 2014, doi: 10.1039/C3IB40221E.

[91] L. Sardelli, D. P. Pacheco, L. Zorzetto, C. Rinoldi, W. Święszkowski, and P. Petrini, "Engineering biological gradients," *Journal of Applied Biomaterials and Functional Materials*, vol. 17, no. 1. SAGE Publications Ltd, Jan. 01, 2019. doi: 10.1177/2280800019829023.

[92] E. Oragui, "The Role of Bioreactors in Tissue Engineering for Musculoskeletal Applications," *Open Orthop J*, vol. 5, no. 1, pp. 267–270, Aug. 2011, doi: 10.2174/1874325001105010267.

[93] A. Bar, E. Ruvinov, and S. Cohen, "Live imaging flow bioreactor for the simulation of articular cartilage regeneration after treatment with bioactive hydrogel," *Biotechnol Bioeng*, vol. 115, no. 9, pp. 2205–2216, Sep. 2018, doi: 10.1002/bit.26736.

[94] Y. Reinwald and A. J. el Haj, "Hydrostatic pressure in combination with topographical cues affects the fate of bone marrow-derived human mesenchymal stem cells for bone tissue regeneration," *J Biomed Mater Res A*, vol. 106, no. 3, pp. 629–640, Mar. 2018, doi: 10.1002/jbm.a.36267.

[95] F. Zhao and T. Ma, "Perfusion bioreactor system for human mesenchymal stem cell tissue engineering: Dynamic cell seeding and construct development," *Biotechnol Bioeng*, vol. 91, no. 4, pp. 482–493, Aug. 2005, doi: 10.1002/bit.20532.

[96] J. Zhang *et al.*, "Perfusion-decellularized skeletal muscle as a three-dimensional scaffold with a vascular network template," *Biomaterials*, vol. 89, pp. 114–126, May 2016, doi: 10.1016/j.biomaterials.2016.02.040.

[97] A. G. Garcia *et al.*, "Multi-scale approach to reconstruct a bioartificial system of system: The example of the bone-tendon-muscle continuum," *2018 13th System of Systems Engineering Conference, SoSE 2018*, pp. 408–410, Aug. 2018, doi: 10.1109/SYSOSE.2018.8428779.

[98] K. P. Krafts, "Tissue repair: The hidden drama," *Organogenesis*, vol. 6, no. 4, p. 225, Oct. 2010, doi: 10.4161/ORG.6.4.12555.

[99] S. Roumeliotis, A. Roumeliotis, E. Dounousi, T. Eleftheriadis, and V. Liakopoulos, "Biomarkers of vascular calcification in serum," in *Advances in Clinical Chemistry*, Academic Press Inc., 2020. doi: 10.1016/bs.acc.2020.02.004.

[100] V. Salvatore, G. Teti, S. Focaroli, M. C. Mazzotti, A. Mazzotti, and M. Falconi, "The tumor microenvironment promotes cancer progression and cell migration," *Oncotarget*, vol. 8, no. 6, pp. 9608–9616, 2017, doi: 10.18632/oncotarget.14155.

[101] D. J. Tschumperlin, "Fibroblasts and the ground they walk on," *Physiology*, vol. 28, no. 6. American Physiological Society, pp. 380–390, Nov. 01, 2013. doi: 10.1152/physiol.00024.2013.